Chapter 3: Optimization of the contour beam gain cost function

The method of optimization of the far-field by changing the reflector surfaces of the DOSR will be dealt with in Chapter 3. The calculation of the cost function, that is the function that gets minimized during synthesis, is described in paragraph 3.1. The global and local search techniques used to minimize this function are introduced in paragraph 3.2. In this paragraph the advantages and disadvantages of global and local search techniques for this application are also discussed. The two methods used to implement the global and local search are the genetic algorithm and the steepest gradient solver. The steepest gradient solver is implemented following [11] but the genetic algorithm has been implemented for the first time in this particular reflector synthesis problem. Both were used individually in some beam syntheses and also used in combination in other syntheses. The synthesis example shown in paragraph 3.3 is an example where the genetic algoritm is used to find an approximate solution and the steepest gradient solver is then used to 'smooth' the contour coverage.

3.1. Cost function

In the diffraction synthesis procedure the objective is to minimize a cost function of the form

$$\Psi = \sum_{j=1}^{M} \left| G_j - GD_j \right|^2 \tag{3.1}$$

where G_j is the actual antenna gain in the j direction and GD_j the desired gain. The actual gain is found from the calculation of the far-field using the methods discussed in Chapter 2 at a specific vector using Equation (2.67) and (2.75) for the p-series method. The desired gain is found from a u-v-space gain template described in paragraph 3.3. To search for this minimum several local and global optimization techniques were examined during the course of this study.

3.2. Optimization methods

The distinction between local and global search techniques is that the local techniques produce results that are dependent on the starting point or initial guess while global methods are largely independent of the initial conditions. In addition, local techniques tend to be tightly coupled to the solution domain. This tight coupling enables the local methods to take advantage of the solution space characteristics resulting in relatively fast convergence to a local maximum [17].

The global techniques, on the other hand, are largely independent of the solution domain. Global techniques are much better at dealing with solution spaces having discontinuous or non-differentiable cost functions, constrained parameters, and/or a large number of dimensions with many potential local maxima.

The genetic algorithm (GA) is classified as a Global or Stochastic technique [18]. GA's are much less likely to get stuck on local minimums. The GA is robust and has a better chance of yielding the global optimum although no optimization technique can guarantee this [11]. The disadvantage to the global method's general independence from the solution space is that it does not use information on local solution space characteristics such as gradients during the search process resulting in generally slower convergence than the local techniques.

3.2.1. The Steepest Gradient Solver

A steepest gradient solver was used to minimize the cost function Ψ in Equation (3.1). When Ψ is minimized the mean square difference between the gain desired and the gain achieved is minimized.

Following [20] the set of surface expansion coefficients CD_i that minimizes Ψ in Equation (3.1) were found by considering

$$\begin{bmatrix} CD_1(k+1) \\ CD_2(k+1) \\ \vdots \\ CD_N(k+1) \end{bmatrix} = \begin{bmatrix} CD_1(k) \\ CD_2(k) \\ \vdots \\ CD_N(k) \end{bmatrix} - \mu \begin{bmatrix} \frac{\partial \psi}{\partial CD_1}\Big|_{CD_1 = CD_1(k)} \\ \frac{\partial \psi}{\partial CD_2}\Big|_{CD_2 = CD_2(k)} \\ \vdots \\ \frac{\partial \psi}{\partial CD_N}\Big|_{CD_N = CD_N(k)} \end{bmatrix} \tag{3.2}$$

where μ is a scale factor. By properly choosing μ , Ψ is minimized since the gradient term on the right hand side in Equation (3.2) gives the direction in the M-dimensional space that results in the greatest increase in Ψ. In practice μ is initially set equal to the inverse of the magnitude of the gradient in Equation (3.2) and is reduced by a factor of 0.9 each time the cost function increases.

The obvious disadvantage of the steepest gradient solver is the required differentiation of the cost function in terms of the surface expansion coefficients. This was done numerically such that a very fast algorithm is needed for the calculation of far-field at the desired vectors or the synthesis process would be extremely slow. During the synthesis process the steepest gradient method was used after the genetic algorithm found a relatively good solution. The final 'smoothing' of the contours over the service area is done using a steepest gradient solver.

3.2.2. The Genetic Algorithm Solver

A GA is a stochastic search procedures modeled on the Darwinian concepts of natural selection and evolution. A set or population of potential solutions is caused to evolve toward a global optimal solution. Simple recombination and mutation of existing solution characteristics. Evolution is the result of selective pressure exerted by fitness based selection [18].

When implementing a GA, a population set of trial solutions is first set up. The chromosome of each solution is consists of a string of genes each coded to form a trial solution vector. Each gene represents a parameter of the fitness. Chromosomes can be entirely encoded (usually binary), floating point or mixed binary and floating point. The following are examples of a chromosomes containing 6 genes in binary coded, and 7 genes in floating point vector form respectively.

{101001,01110,110101,011010,011,10101}

{425,-0.179,120,-537,4652,11.433,0.067}

A generation is a successively created population or a GA iteration. Each current generation contains parents or members of the current generation. A child is member of the generation following on the current generation. To each parent a positive fitness

number is assigned representing a measure of goodness. A reproduction scheme is implemented where genetic material of pairs chromosomes is mixed. This can be performed at crossover points randomly generated for each gene. A mutation is performed on the population where a random changeover of bits (in the case of a binary encoding scheme) is made throughout the population. After this a fitness evaluation is performed on each member of the next generation and a ranking of the total population is made. Based on the ranking some members of the population are discarded. This process is repeated until a cost function level is achieved or a certain number of iterations is exceeded. Certain variations on the basic GA can be implemented, for example tournament selection, where "N" individuals at randomly selected from the population and the individual with highest fitness value in group is then selected. This is different from the proportionate selection that was described earlier. Another variation in the basic GA is the use of elitism. In a simple GA the most fit individual may not survive. Elitism saves the fittest individual and places it in next generation. Simple GA is generational; that is the new generation completely replaces old generation. Steady-state GA has overlapping generations. In a steady state GA a percentage of current generation gets replaced with newly created individuals. There are various methods of choosing which individuals to replace for example worst individuals, random replacement or parents. The steady-state GA can in some cases increase convergence.

Many factors influence convergence but the number of trial solutions and the percentage random mutation were the most important. Rapid convergence didn't always lead to the best solution.

The genetic algorithm is a domain independent, global optimization method that is simple to implement and very good results were achieved using these kind of optimizers.

During the synthesis process a genetic algorithm is used on the logarithm of the surface expansion coefficients. Restrictions are placed on the initial generation and further mutation of the chromosomes of the solution to prevent inflection areas (areas where the second derivative changes sign) on the subreflector. For this specific example the subreflector surface expansion is made on a surface with a projected circular aperture of 20 wavelengths as shown in Figure 12. The diameter of the projected aperture of

surface of the subreflector expansion is determined by ray tracing the main reflector edge rays from the maximum required scanned positions of the beam footprint to the focal region and choosing a diameter that overlaps the furthest subreflector rim points. The subreflector size and the projected area on which the expansion is made is therefore determined by the required scan width. For the example in Chapter 5 where the surface is described in terms of a mechanical finite element matrix the optimization parameters are the actuator amplitudes (or control voltages) and the Modified Jacobi polynomial description of the surface is only used to get initial values for the actuator amplitudes.

3.3. Design of a CONUS beam

A CONUS beam was designed using a Cassegrain dual offset reflector antenna with the following parameters for the unshaped surfaces:

Wavelength: 0.025

Main reflector focal length F : 72.639 wavelengths

Main reflector aperture D : 60 wavelengths

Main reflector offset y_c : 55.76 wavelengths

Subreflector tilt angle β_s : 14.32°

Subreflector eccentricity e : 2.879

Subreflector half interfocal distance c : 14.596 wavelengths

Feed tilt angle α : -29.07 °

Subreflector orientation α_s : 0°

β_s : -14.32 °

γ_s : 0°

Subreflector offset from main coordinate origin S_x : 0 wavelengths

S_y : -55.76 wavelengths

S_z : 0 wavelengths

Feed offset from unshaped focal point x_f : 0 wavelengths

y_f : 0 wavelengths

z_f : 0 wavelengths

Feed orientation α_f : 0°

β_f : -29.07 °

γ_f : 0°

Feed edge illumination level : -10 dB

Feed edge illumination angle: 12°

Subreflector oversizing factor: 1.2

Figure 17 shows the required surface deviation contours from the unshaped surfaces to produce a CONUS beam. Figure 18 shows the u-v space template and Figure 19 shows the achieved normalized coverage for the CONUS beam. The peak co-polarized gain was 34.57 dBi with a peak cross-polarized gain of 0.61 dBi.

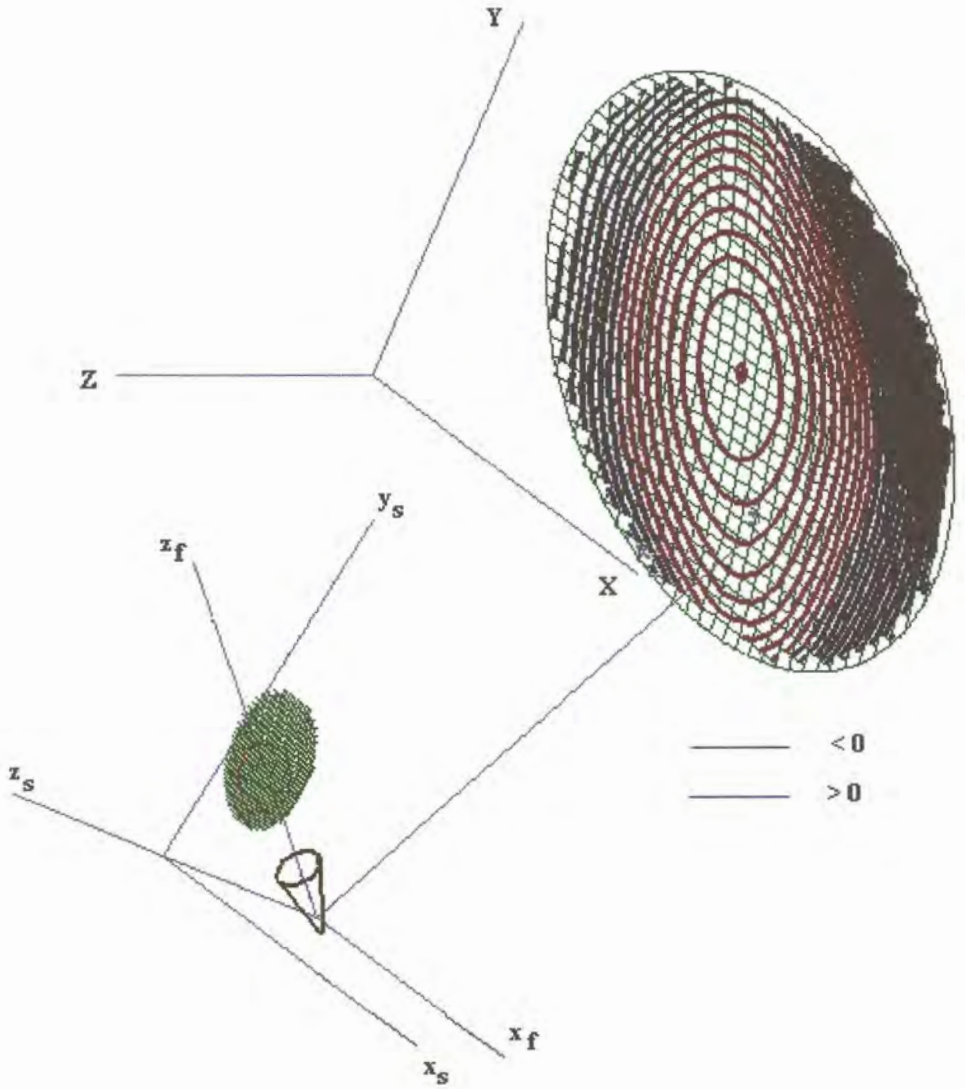

Figure 17. Required main and subreflector surface deviation in 1mm contour intervals for CONUS type contour beam.

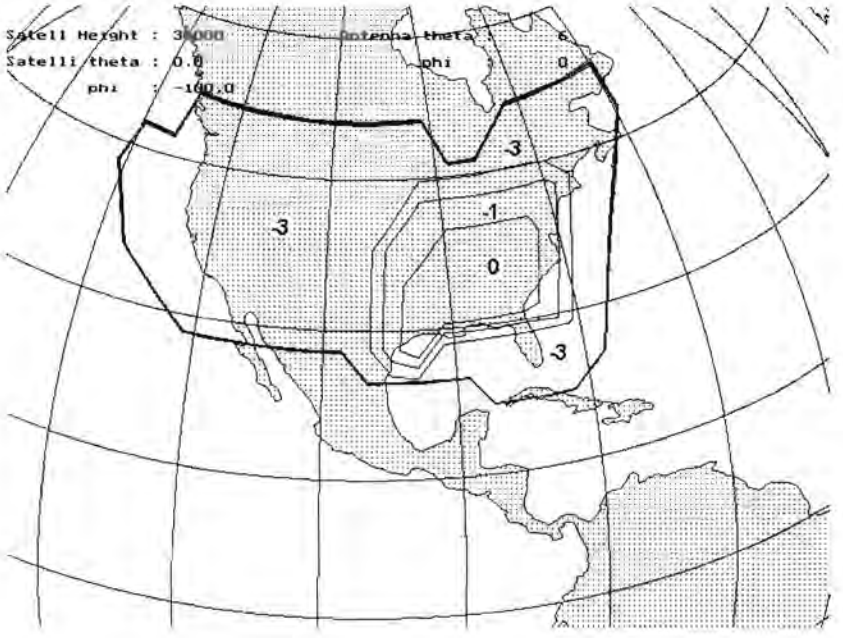

Figure 18. Template used to calculate cost function during synthesis of the CONUS beam.

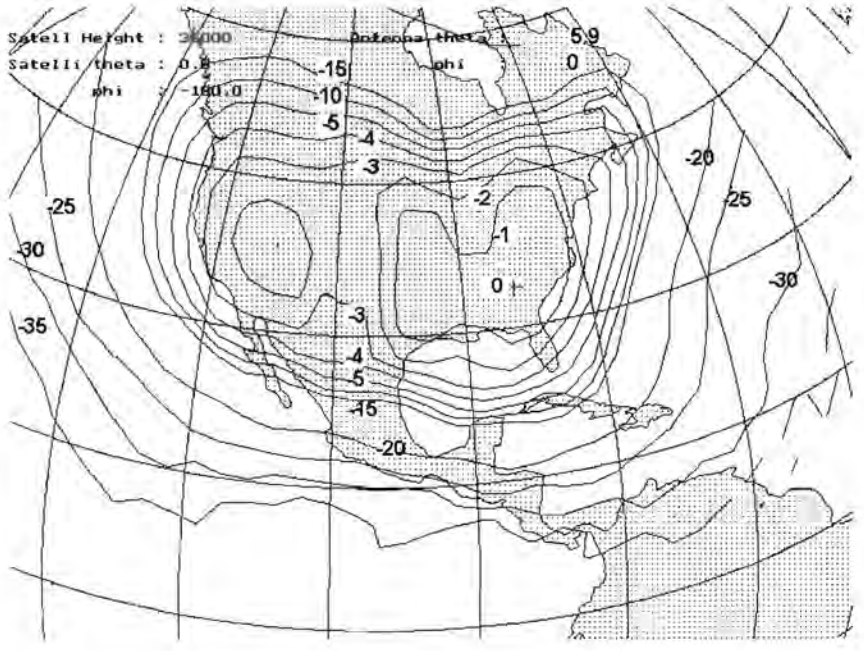

Figure 19. CONUS beam generated using combination of genetic and steepest gradient solvers in synthesis algorithm.

From Figure 19 the gain for the different gain regions can be seen to be achieved satisfactorily and comparison with the results in [11] also shows good agreement in terms of gain and cross polarization performance. This and other examples give confidence that the optimization routines are behaving as expected. The solutions obtained using steepest gradient solver are not always optimum and sometimes 'get stuck' in a local minimum. Operator intervention is required to get the coefficients in the Modified Jacobi polynomial series to the approximate values to ensure convergence and this seems to be acquired only through experience and the knowledge of what coefficients control what characteristics on the surface. Setting the lowest mode coefficients (C_{01}, C_{02}, C_{10} and D_{01} , D_{02} in Equation 2.134) to particular initial values seems to ensure a faster and better convergence. The genetic solver gives a good approximate solution within a reasonable time but seems to be unable to do a final convergence on the particular minimum. In the example shown a genetic solver is used to get an approximate solution and the steepest gradient solver is used to 'smooth' the footprint contours. In the following chapters the implementation of the mechanical finite element description of the surfaces into the diffraction synthesis code will be shown.

Chapter 4: Mechanical design of the dual reflector antenna

In Chapter 4 the mechanical properties of thin sheets are discussed and the set of differential equations governing their shape under different forces is shown. The first part of this dissertation simply examined the electromagnetic performance for a reconfigurable DCBR antenna. Next, the mechanical aspects of the design will be included. The feasibility of this antenna has been demonstrated by a practical mechanical design using piezoelectric adjustable linear actuators. This design is based on a mechanical finite element analysis of four prototype surfaces and a subsequent actuator placement study. In this study, the main reflector was assumed to be fixed and an adjustable subreflector surface was designed using a flexible material called Lexan. An actuator placement study was performed on materials with various stiffnesses to determine the suitability for this application by the smart structures division of the mechanical engineering department of The Ohio State University. A design was done using diffraction synthesis (shaping) on the main reflector and subreflector to produce a contiguous United States (CONUS) beam from a geostationary satellite position in its normal or undeformed mode. In this design, the main reflector and subreflector were shaped to produce the contour beam as was previously shown. A set of other coverage samples were chosen to study the ability to achieve coverage by mechanically unconstrained adjustment of the subreflector surface. A geographical area with comparable size but different shape was used first. Next a case requiring a smaller coverage area was evaluated. Brazil and South Africa were used as examples for these two studies. These subreflector surfaces were assumed as typical in terms of amplitude and size and an actuator placement study was performed using commercially available mechanical finite element code. The actual achievable mechanical surfaces were then used to evaluate the subsequent radiation pattern performance.

4.1. Mechanical description of surfaces using shell elements

Mechanically, the shape of the antenna is governed by a set of differential equations given by

$$\frac{\partial}{\partial\xi}\{\alpha_\eta N_\xi\}+\frac{\partial}{\partial\eta}\{\alpha_\xi N_{\eta\xi}\}+\frac{\partial\alpha_\xi}{\partial\eta}N_{\xi\eta}-\frac{\partial\alpha_\eta}{\partial\xi}N_\eta+\alpha_\xi\alpha_\eta\left(\frac{O_\xi}{R_\xi}+q_\xi\right)=0 \quad , (4.1)$$

$$\frac{\partial}{\partial\xi}\{\alpha_\eta N_{\xi\eta}\}+\frac{\partial}{\partial\eta}\{\alpha_\xi N_\eta\}+\frac{\partial\alpha_\eta}{\partial\xi}N_{\eta\xi}-\frac{\partial\alpha_\xi}{\partial\eta}N_\xi+\alpha_\xi\alpha_\eta(\frac{Q_\eta}{R_\eta}+q_\eta)=0\,, \quad (4.2)$$

$$\frac{\partial}{\partial\xi}\{\alpha_\eta Q_\xi\}+\frac{\partial}{\partial\eta}\{\alpha_\xi Q_\eta\}-\alpha_\xi\alpha_\eta\{\frac{N_\xi}{R_\xi}+\frac{N_\eta}{R_\eta})+\alpha_\xi\alpha_\eta q_\zeta=0 \quad , \quad (4.3)$$

$$\frac{\partial}{\partial\xi}\{\alpha_\eta M_\xi\}+\frac{\partial}{\partial\eta}\{\alpha_\xi M_{\eta\xi}\}+\frac{\partial\alpha_\xi}{\partial\eta}M_{\xi\eta}-\frac{\partial\alpha_\eta}{\partial\xi}M_\eta-\alpha_\xi\alpha_\eta(Q_\xi-m_\xi)=0\,, \quad (4.4)$$

$$\frac{\partial}{\partial\xi}\{\alpha_\eta M_{\xi\eta}\}+\frac{\partial}{\partial\eta}\{\alpha_\xi M_\eta\}+\frac{\partial\alpha_\eta}{\partial\xi}M_{\eta\xi}-\frac{\partial\alpha_\xi}{\partial\eta}M_\xi-\alpha_\xi\alpha_\eta(Q_\eta-m_\eta)=0 \quad (4.5)$$

where the α's are defined as the scaling factor, M is defined as the stress couple, N is the stress resultant, Q is the transverse shear stress resultant m is the moment load and q is the surface load. For certain shell shapes and actuation strategies equations (19-23) can be solved in closed form [20]. In this study, however, the solution was found by employing finite element analysis on the curved structure. In order to accomplish this task, 3600 (8 node) shell elements were used to discretize the reflector. The shell elements were configured to form the subreflector shape needed for the initial required geographical coverage area. Whenever a different shape is needed, high deflection piezoelectric actuators are utilized to force a new shape. In this case twenty three high deflection actuators were mounted at various points on the structure as shown in Figure 20. Note that the black dots represent actuator attachment locations on the internal surface. They were divided into 16 on the internal surface and 7 located at discrete points along the perimeter. Each actuator is made up of a stack of high deflection piezoelectric wafers called Rainbows as shown in Figure 21. A single wafer is dome shaped and capable of a deflection of about 0.5 mm. The equations that were utilized in modeling the deflection emanating from the Rainbows can be found in Reference [21]. To increase the deflection of an actuator comprised of these wafers, the wafers were placed in a clamshell configuration as shown in Figure 22. The actuator that is utilized in this study consists of a stack of 40 Rainbow actuators with a 2 inch diameter. This means that a clamshell stack of 40 is capable of about 2.0 cm of deflection.

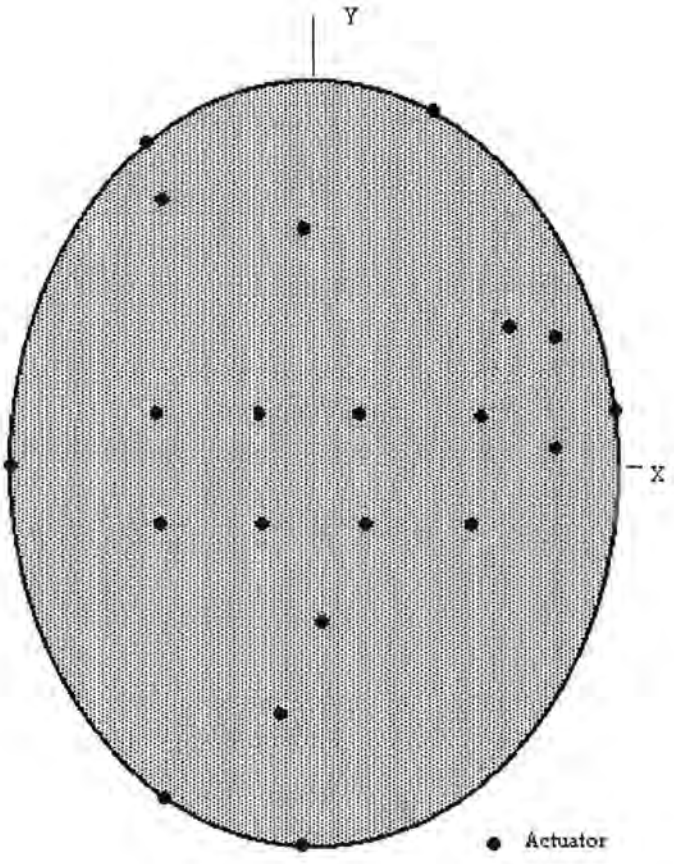

Figure 20. Actuator positions projected on the x_s-y_s plane.

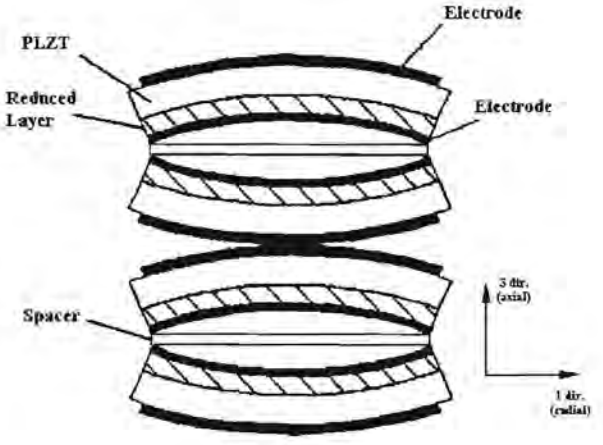

Figure 21. Showing individual stack showing clamshell configuration

The actuators are mounted to a rigid back surface. The flexible reflector is then draped over the actuators and the actuator ends are attached to the surface via epoxy. Spacers are used between the back surface and the actuator to ensure the proper height.

Actuator placement was done by examining a family of possible shapes and placing the actuators in locations that will produce these desired shapes. While this methodology is fast and effective, there are some shapes that a finite amount of actuators will not be able to achieve. This was not a major concern for two reasons: First, most required geographical coverage can be achieved using simple elliptically shaped beams oriented as needed. This eliminates some antenna shapes and some actuators. Second, the antenna can be designed based on all possible footprints that will likely be needed in the forseeable future. In addition, having too many actuators increases surface control complexity and thereby increases cost.

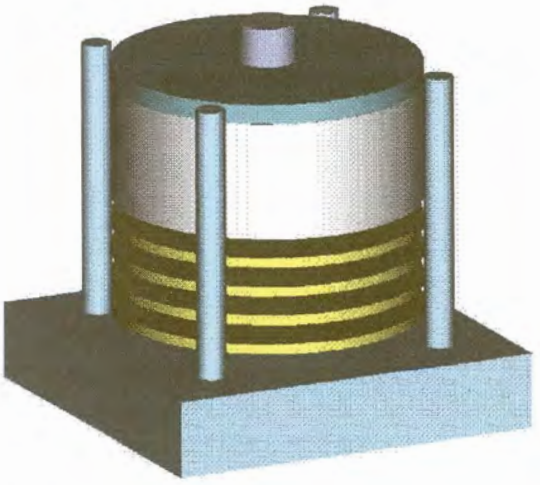

Figure 22. Rainbow actuators in stacked clam configuration.

4.2. Diffraction synthesis results and mechanical design performance

Three examples have been implemented to test the achievable accuracy of the surface after the mechanical design was completed. In the first example, a CONUS beam is synthesized for a geostationary position at 100°W. This done by optimizing 54 main- and subreflector surface expansion coefficients and three quantities associated with the feed position. A steepest gradient solver in combination with a genetic solver was used and achieved comparable results. Different designs were implemented to study the relation between beam scan angle, the required subreflector size and the ease of synthesis. A Cassegrain DCBR antenna with an aperture of 60 wavelengths was used. After the optimization for the CONUS beam, the main reflector surface is assumed to be fixed and all other beams were generated by only adjusting the surface of the subreflector. In this case no feed adjustment was made. This simulates a realistic implementation for an actual satellite antenna where it may not be easy to have an adjustable feed due to rigid RF components. Figure 18 shows the u-v space template and Figure 19 the achieved normalized coverage for the CONUS beam. The peak co-polarized gain was 34.57 dBi with a peak cross-polarized gain of 0.61 dBi. Figure 25 shows the achievable subreflector surface and the resulting co-polarized radiation footprint.

Next, the subreflector surface was adjusted to achieve a beam covering a geographical region of comparable size but of different shape and required gain. Brazil was selected from a geostationary position of 50°W. Figure 23 shows the antenna radiation footprint and the required deviation from the initial hyperboloid surface in 2 mm contour intervals. In this case no feed adjustment was made. Figure 26 shows the mechanically achievable surface and the calculated co-polarized radiation footprint for the adjusted actuators.

As a third test the subreflector surface was adjusted to achieve a beam covering Southern Africa from a geostationary position at 5°E. Figure 24 shows the antenna radiation footprint and the required deviation from the initial hyperboloid surface in 2

mm contour intervals. Figure 27 shows the mechanically achievable surface and the calculated co-polarized radiation pattern.

For the mechanical design a stationary feed constriction was assumed but two further diffraction syntheses were made adjusting the feed in the subreflector mother surface symmetry axis direction (z_s) and in the (x_s -y_s) plane. This reduced the required maximum surface deviation from 22mm to 12mm. The ability to adjust the feed gives a large degree of freedom in contour beam synthesis but may not be practical in many cases due to the rigidity of the feed network elements.

The feasibility of a practical reconfigurable contour beam antenna using a dual offset reflector configuration with an adjustable subreflector surface has been showed by a practical design of an adjustable surface. The next and most important step is to develop synthesis procedure incorporating a mechanical finite element (FEM) model using shell elements. This will be shown in the next section.

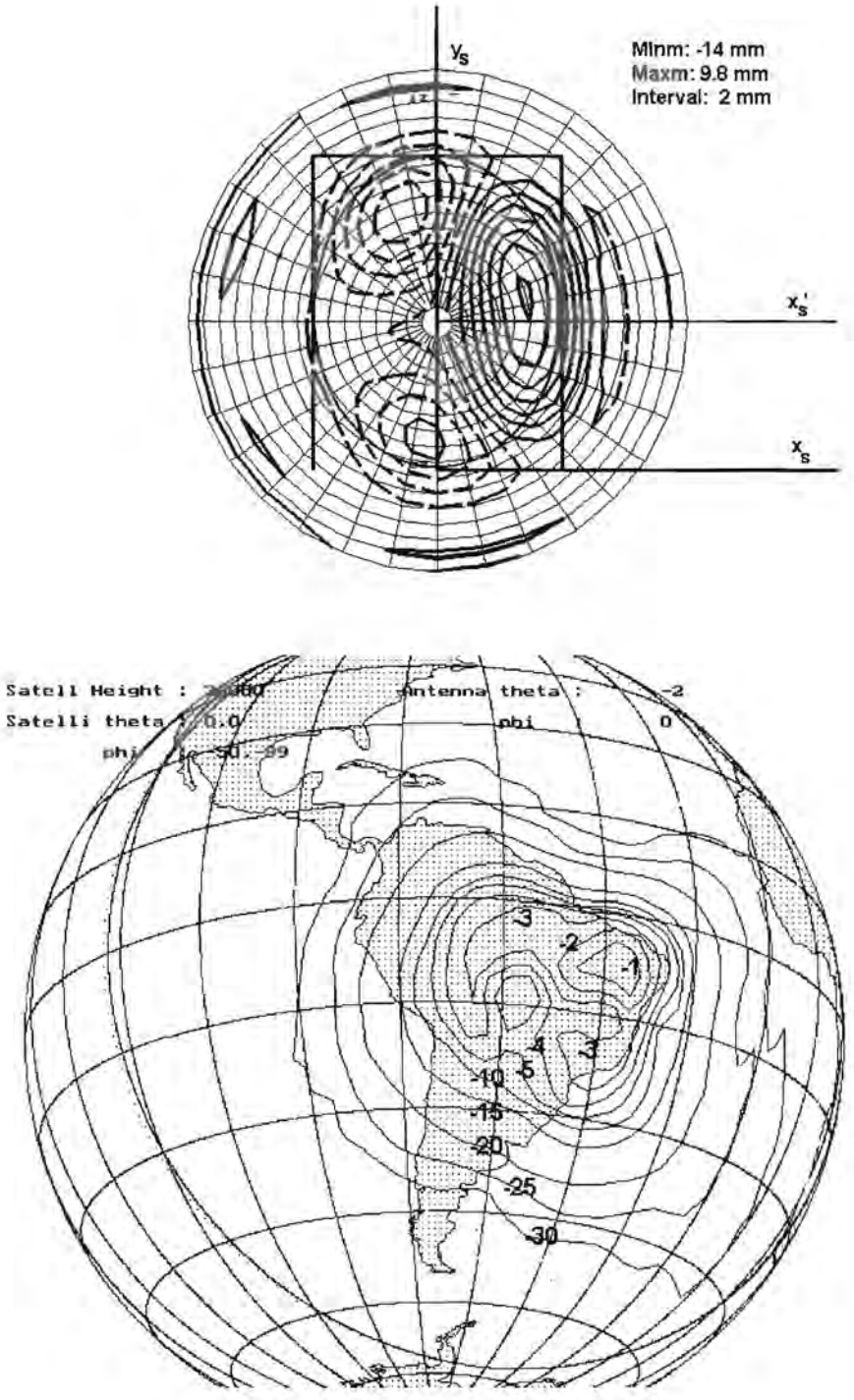

Figure 23. Required deviation from the initial hyperboloid surface in 2 mm contour intervals and the calculated co-polarized antenna radiation footprint for case 2.

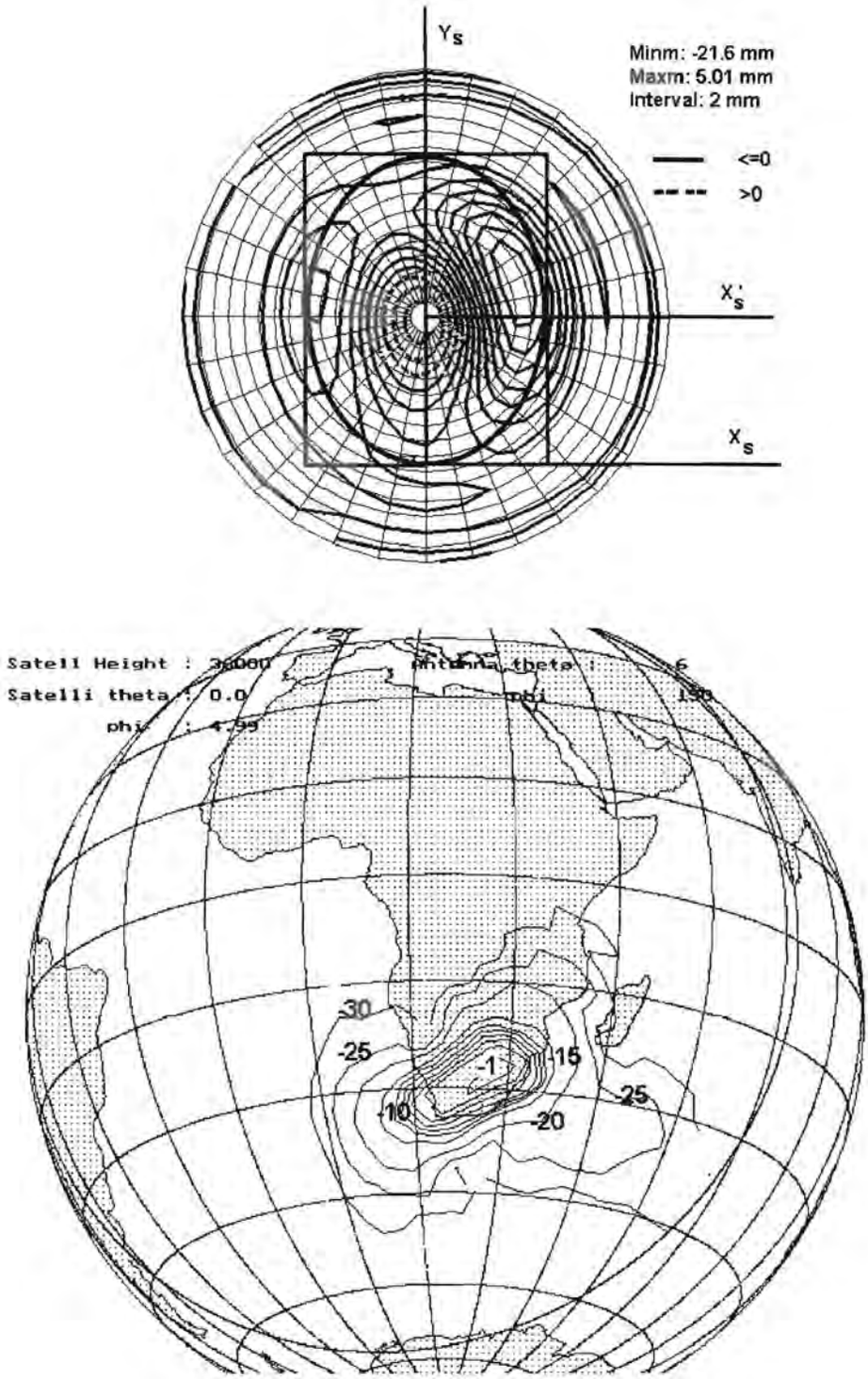

Figure 24. Required deviation from the initial hyperboloid surface in 2 mm contour intervals and the calculated co-polarized antenna radiation footprint for case 3.

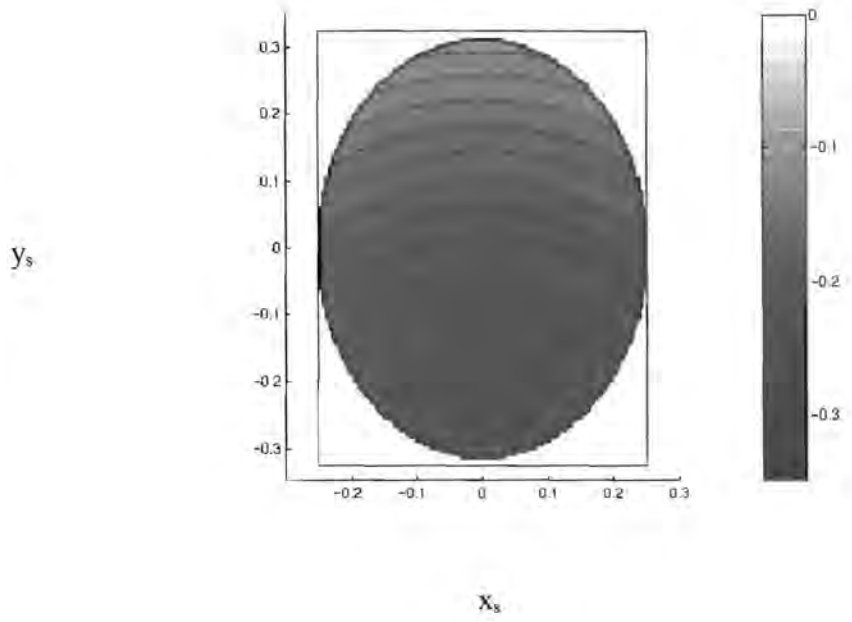

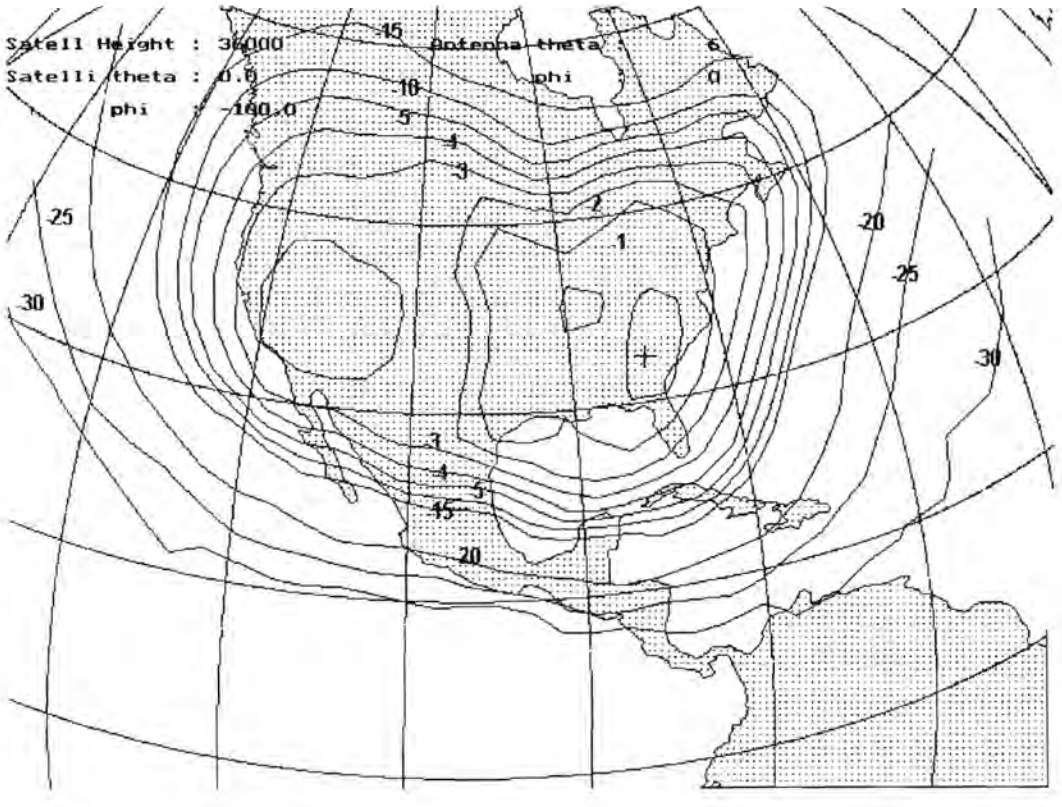

Figure 25. The achievable subreflector surface with no actuator adjustment and the resulting co-polarized radiation footprint.

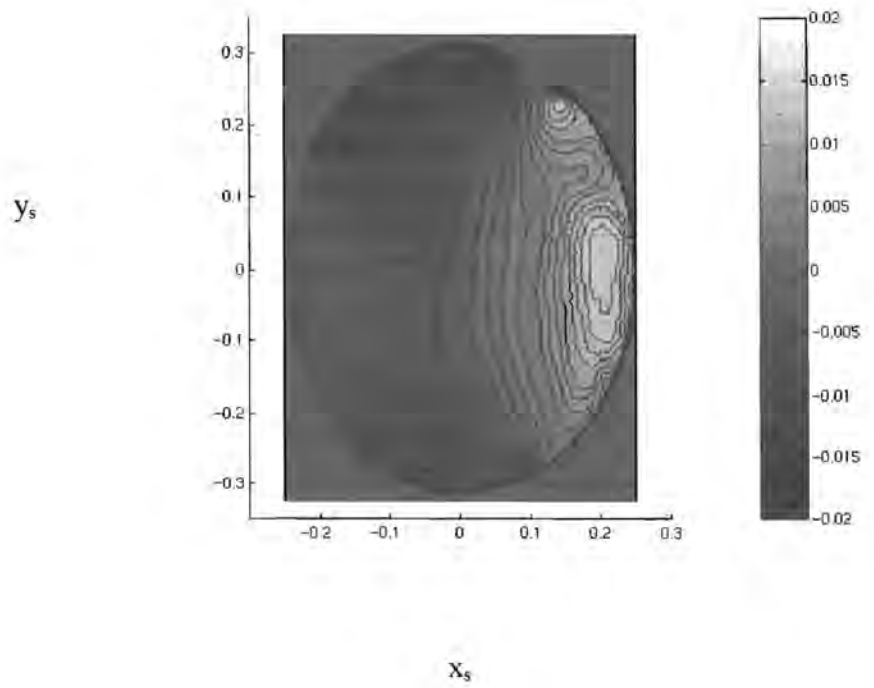

Figure 26. Mechanically achievable surface and the calculated co-polarized radiation pattern for case 2.

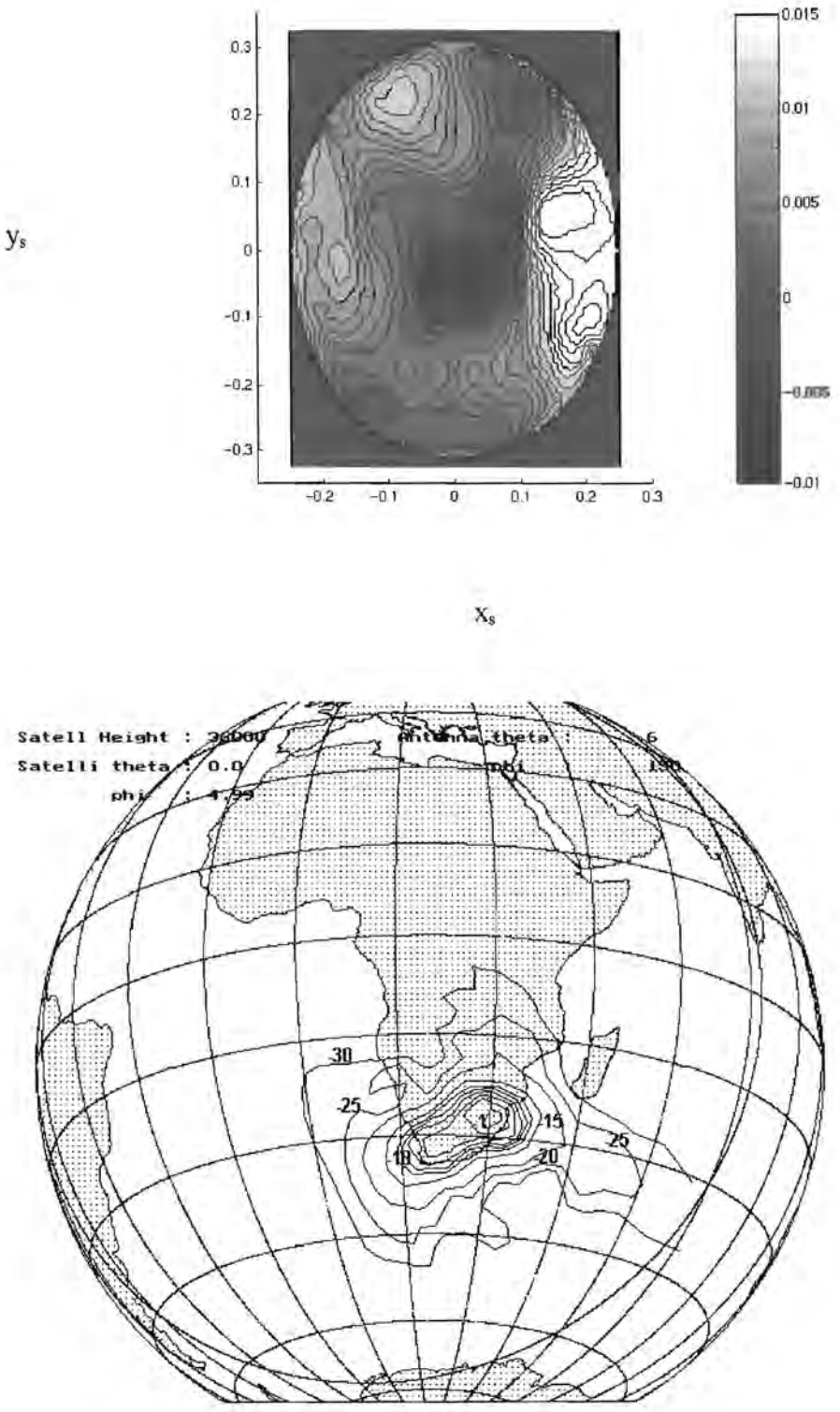

Figure 27. Mechanically achievable surface and the calculated co-polarized radiation pattern for case 4.

Chapter 5: Contour beam synthesis using the mechanical FEM surface description

The diffraction synthesis procedure written by the author was modified to incorporate a mechanical finite element description of the surfaces of the dual reflector antenna. The mechanical FEM unit developed by the Smart Materials and Structures division of the Department of Mechanical Engineering of The Ohio State University by Yoon and Washington, was designed to be compatible with the contour beam synthesis software. The resulting code enables direct synthesis in terms of the exerted actuator forces on a surface with a predefined stiffness matrix as described in the following paragraph.

The code also eliminates the second step of the FEM analysis described in Chapter 4 because the synthesis is now done on mechanically realistic surfaces using the actual actuator positions and displacements. In addition, many iterations can be performed much faster and more conveniently, as opposed to the examples in the previous chapter where essentially only one iteration was done on the mechanical surface. The result is a very useful tool to create a suitable design and predict the performance of the antenna taking into consideration the mechanical properties of the surface materials and the actuators used to reconfigure the antenna.
A new way of adjusting a reflector by bonding piezoelectric strips to a deformable surface was also studied [6] using this software.

5.1. Mechanical FEM diffraction synthesis

The FEM solver, developed in the Delphi RAD object oriented Pascal language by Yoon, was incorporated into to the synthesis software that was described previously in Chapter 2, also developed in Delphi by the author. The surface description of the reflectors (in this case the subreflector) is now made in terms of the actuator amplitudes instead of the modified Jacobi polynomial expansion coefficients used

previously for the examples in Chapter 3. The synthesis software reads the following set of data files:

a. Geometry file: Contains the unshaped main and subreflector parameters and the feed illumination function or feed data file.

b. Node file: Contains the node coordinates of the surfaces.

c. Connectivity file: Contains the connectivity table of the FEM elements.

d. Boundary condition file: Contains the boundary condition vector. This file gets updated at each iteration during the synthesis process.

The FEM code first sets up the global stiffness matrix from the material parameters and the node and connectivity data files. The material parameters are the Young's modulus, the Poison ratio relating form shape change and thickness of the shell elements.

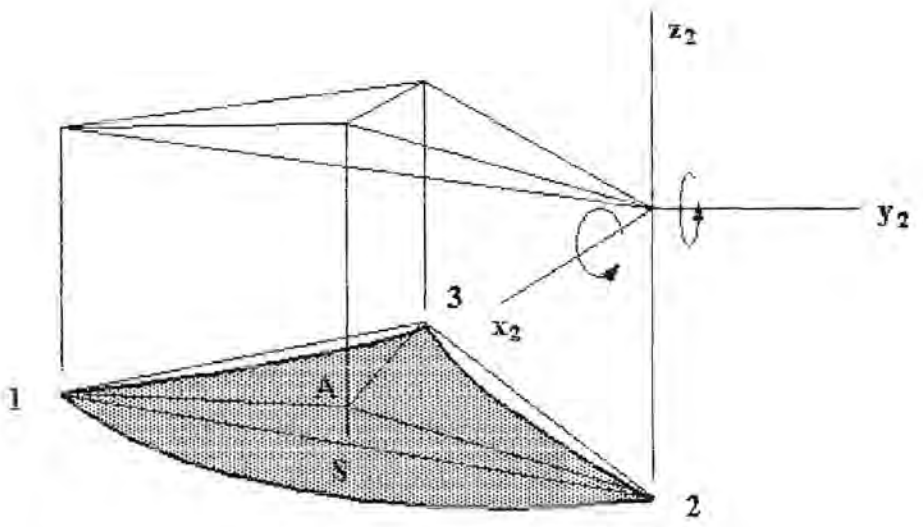

Figure 28. FEM shell element geometry

The stiffness matrix is now used together with the boundary condition file (containing initial actuator displacement values at certain node positions) and solved using a 'forward elimination and back substitution' method. The resultant vector gives the new node positions of the surface. Each element has three nodes as shown in Figure 28. Each node has 5 degrees of freedom namely a node position coordinate and two node rotations due to applied moments at the node.

The position S in Figure 28 is determined by finding position A first. To fall in the plane of points 1,2 and 3 within the area 123 the sum of areas 1A2, 2A3 and 3A1 must

be equal to the area of 123. This fact is used as a test to determine which element contains the specular point. Using the known rotation around any node and the distance 2A the position of S and the normal at S can be found.

The specular point on the subreflector is found as before using the known integration point and feed position and the Newton method with the LU solver. Figure 29 shows the subreflector projection in the x_s - y_s plane and the FEM node- and element positions.

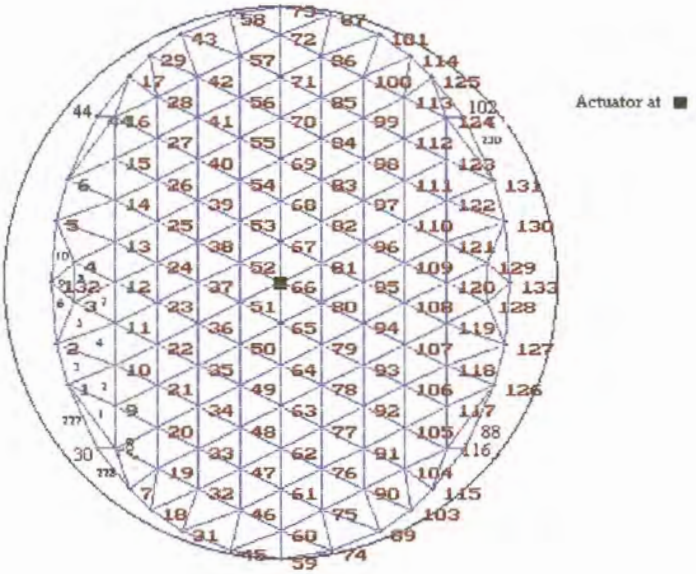

Figure 29. Subreflector projection in the x_s - y_s plane showing the FEM node- and element positions.

Figure 30 shows the surface deviation contours with the actuators at the positions indicated and actuator 66 adjusted to 10 mm for a typical flexible plastic surface 0.05" thick. It can clearly be seen from the contour levels (blue contours are positive and magenta contours are negative) that actuator placement is critical to prevent undesired "buckling" in thin, stiff materials.

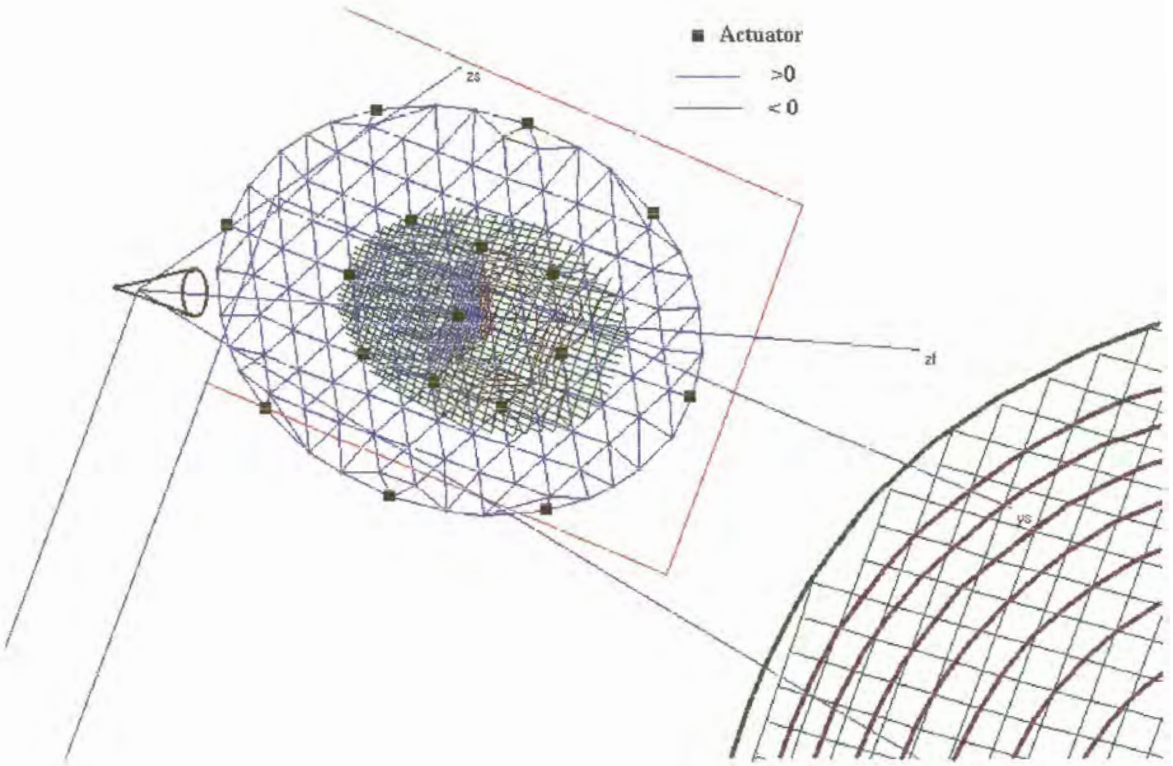

Figure 30. Subreflector surface deviation due to displacement of actuator 66 by 10mm.

This example illustrates that real mechanical implementation issues, for example buckling of the adjustable reflector antenna surface, can now be addressed.

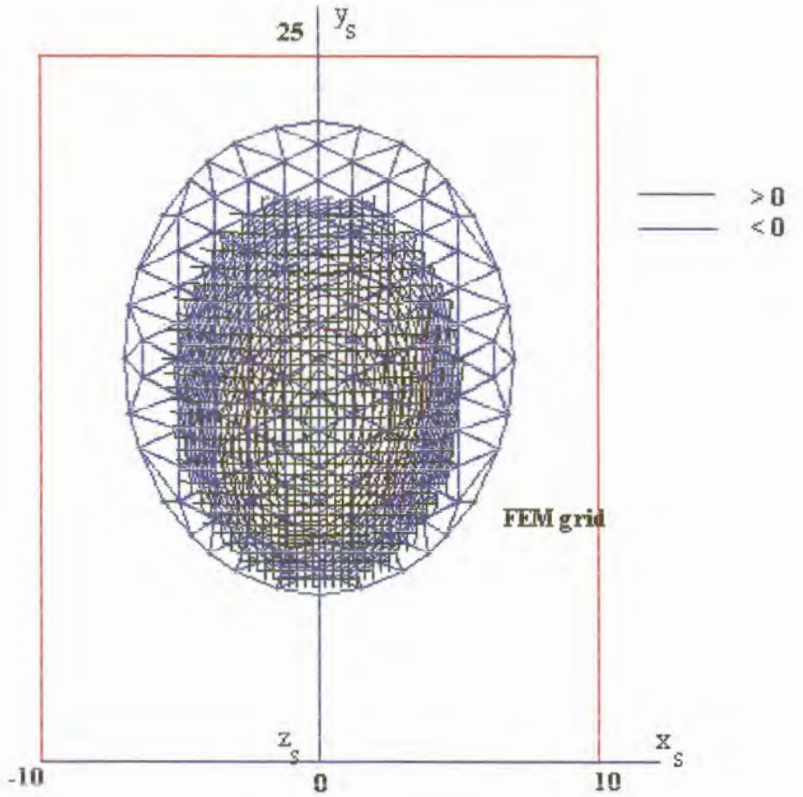

Figure 31. Required surface deviation contours in 1 mm contour intervals for the subreflector surface with an unshaped main reflector giving a cost function of 59.5 units on an elliptical contour beam case.

5.2. The effect of mechanical surface properties on actuator number and placement

In order to determine the minimum number of actuators and where they should be placed a simple elliptical beam shape was synthesized changing the thickness and stiffness of the surface each time for three actuator arrangement patterns. The actuators were placed in equispaced triangular pattern first, then in a rectangular pattern and finally in a radial pattern. These patterns were chosen to make a general study of actuator placement effects as opposed to the case specific placements done before. The following reflector material properties were adjusted: Young's modulus

and material thickness. The Poisson ratio was kept constant at 0.334 which is a typical value for stiff polymers.

As a case study a 7° x 4.5° elliptical beam with the main semi-major axis tilted 45° was used to study the effect of surface material thickness on the required number of actuators. This study determined the minimum number of actuators for a given surface to guarantee a given cost function value. The unshaped cost function value ψ from Equation 3.1 is 149.5 units. Figure 31 shows the required surface deviation for the subreflector with no main reflector shaping that produce a cost function value of 59.5 units. A minimum of 65 is deemed acceptable and the minimum number of actuators that can achieve this value are determined. Figures 32 (a)-(c) show the triangular actuator pattern for three cases with different material thickness with 14, 21 and 39 actuators respectively. In each case the surface material stiffness is kept at a typical constant value for sheet plastic. Figures 33 (a)-(c) show the rectangular actuator pattern for the three material thickness cases with 14, 21 and 39 actuators respectively and Figures 34 (a)-(c) show the actuator arranged along a radial pattern with 8 radials for the three cases with 14, 21 and 39 actuators respectively. The number of actuators are not equal for each of the cases of each example but they are almost the same and for the lower actuator numbers a greater portion of actuators lie in the rim region that do not contribute significantly to the radiation pattern shape.

Table 1 shows the three actuator arrangement patterns and the cost function for each of the surface material thickness. From Table 1 it can be seen that the 0.05" surface needs many actuators to give acceptable performance. Another case is run with 65 actuators arranged in the triangular pattern that achieves the required cost but the actuators have to be spaced with their center lines 3.5 cm apart. In the case of the Rainbow piezoelectric stack this arrangement is impossible but alternative linear actuators may be considered. More control over the surface is achieved in the 0.1" surface thickness case but the best performance for each case is for the 0.3" surface. This use of this surface may be impractical due to the force that the actuators must be able to exert on the surface.

The radial arrangement of the actuators does not make the minimum cost for any case because 8 radial 'spokes' are used. This leaves large areas uncontrollable. This is an issue that needs to be addressed in a design of bonded piezoelectric surfaces to the back of a reflector as proposed in [6].

The performance of the triangular and rectangular actuator arrangements is almost the same with the triangular arrangement slightly better.

Thickness (inch)	Triangular		Rectangular		Radial	
	Number	Cost	Number	Cost	Number	Cost
0.05	16	109.6	15	102.1	14	104.7
	22	93.6	21	96.8	21	93.1
	38	82.1	40	88.1	39	71.8
0.1	16	86.2	15	87.6	14	94.5
	22	74.6	21	79.2	21	73.1
	38	62.2	40	64.2	39	70.1
0.3	16	77.5	15	76.3	14	92.1
	22	64.2	21	67.7	21	69.2
	38	60.1	40	61.6	39	66.1

Table 1. Cost function comparison of actuator number and arrangement for different surface thickness.

This study gives an understanding of the required surface thickness and the number of actuators required to achieve a desired shape. The same procedure needs to be applied if a material of a different stiffness is used. In the next section the experience gained from this study is applied to generate arbitrary antenna radiation footprints.

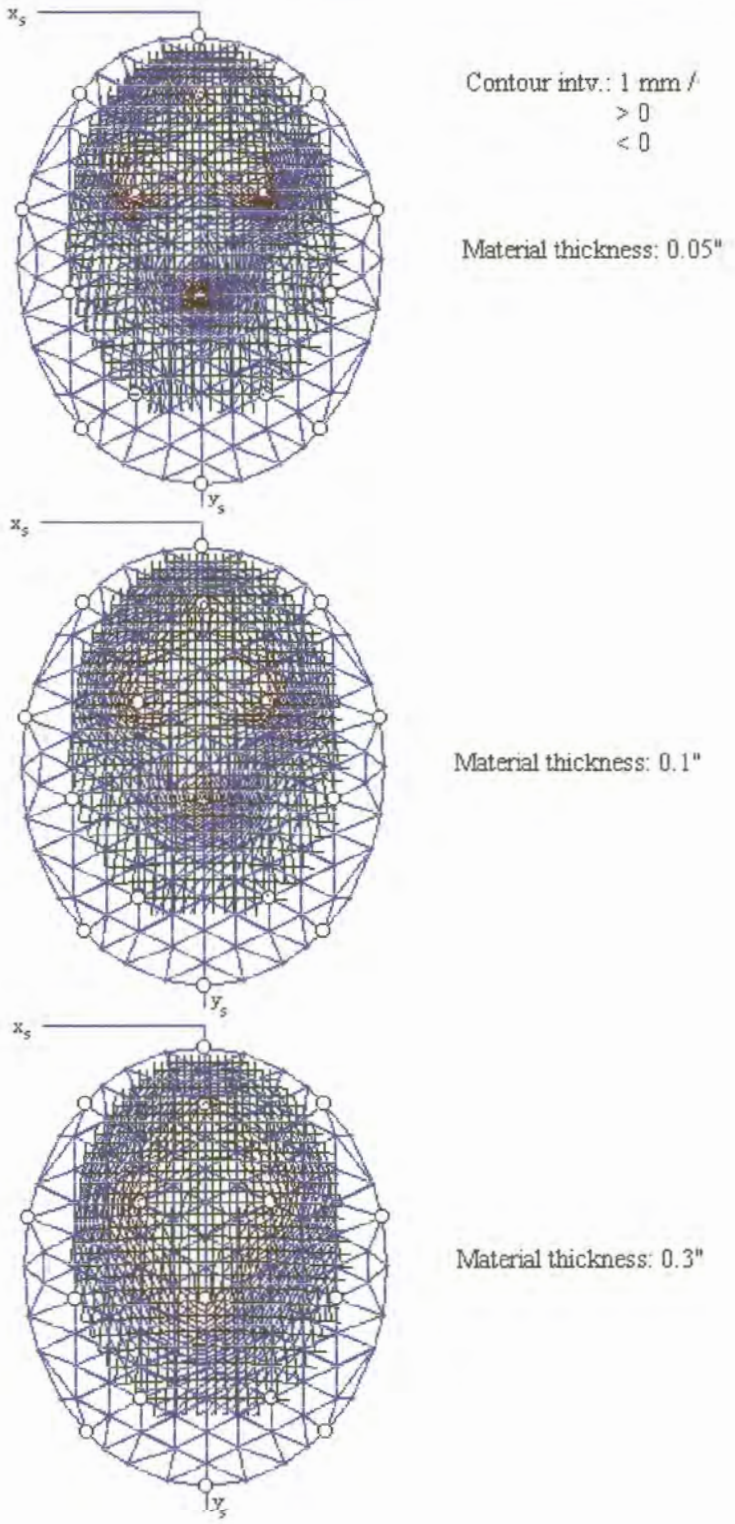

Figure 32 (a) Surface deviation contours for 16 actuators arranged in a triangular pattern and bonded to different surface material thickness of 0.05", 0.1" and 0.3" respectively.

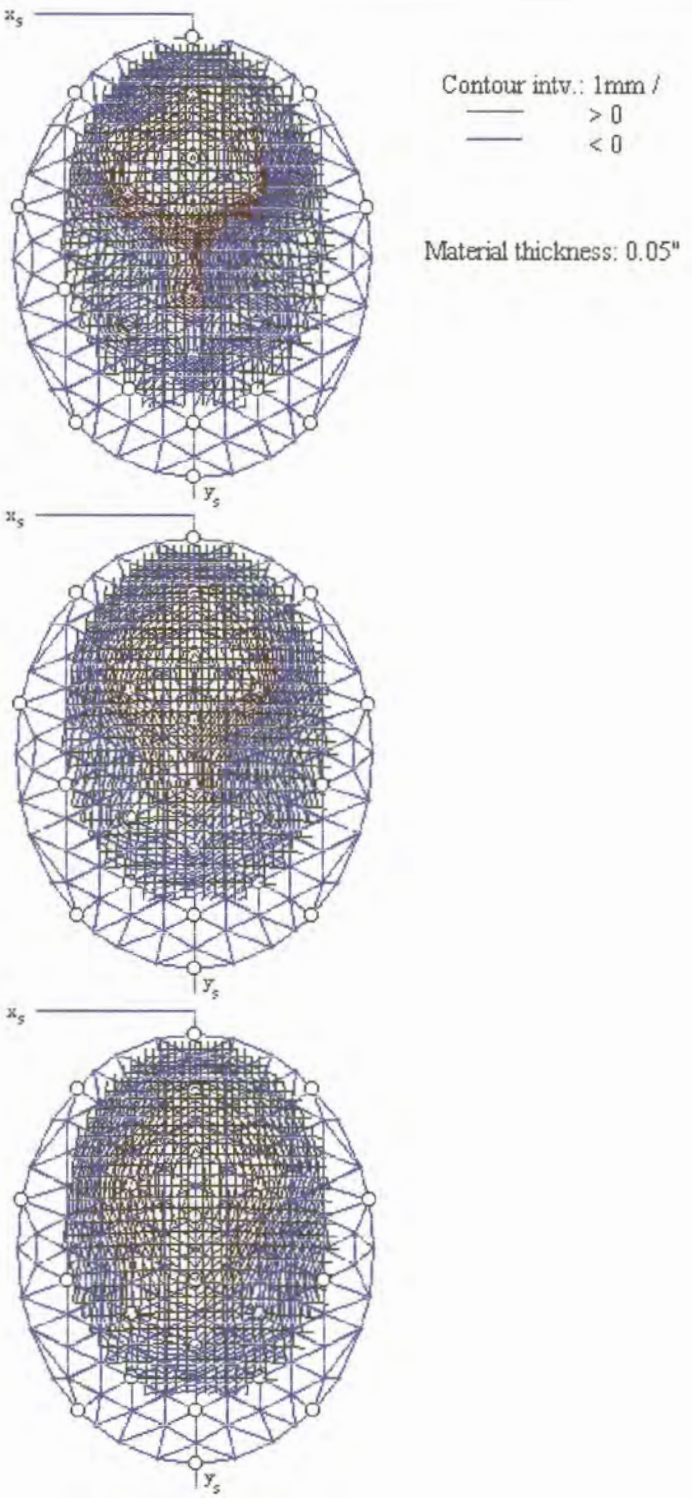

Figure 32 (b) Surface deviation contours for 22 actuators arranged in a triangular pattern and bonded to different surface material thickness of 0.05", 0.1" and 0.3" respectively.

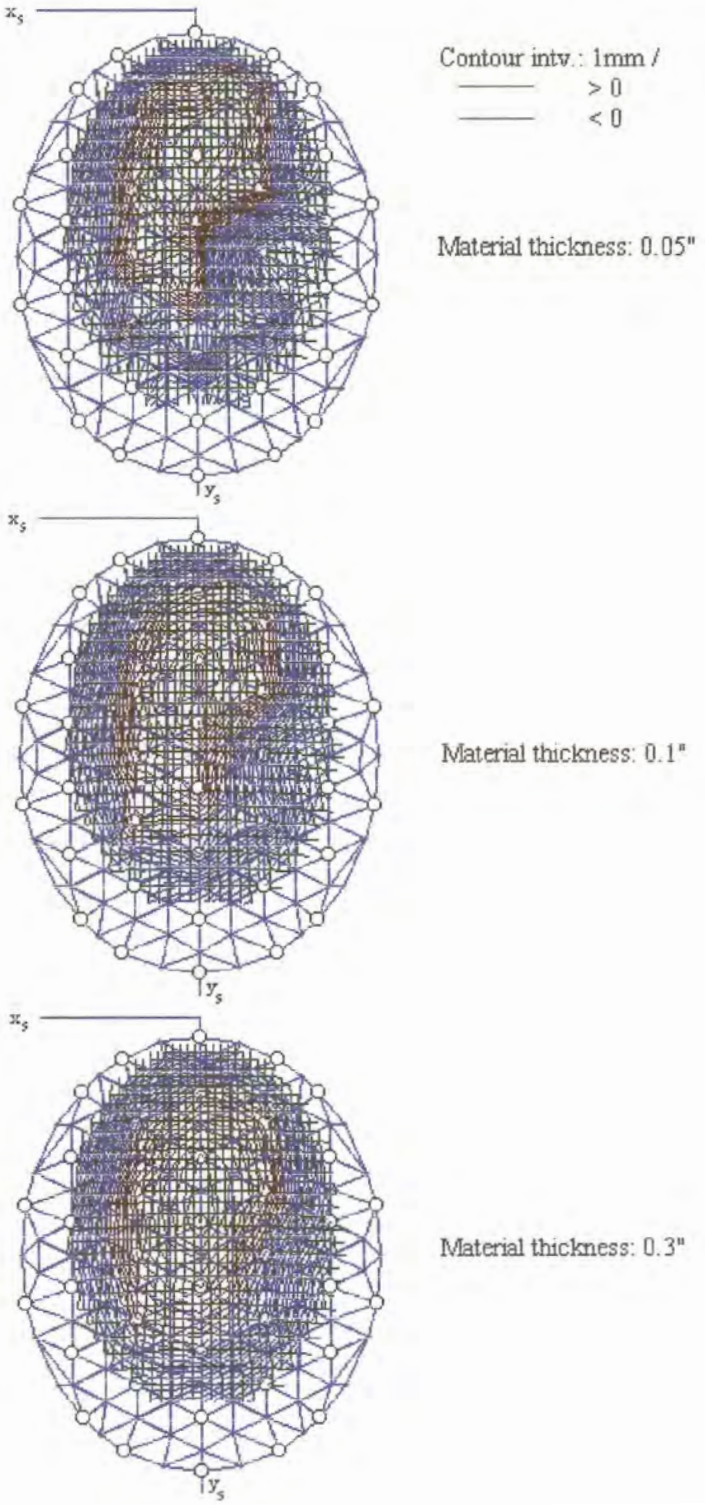

Figure 32 (c) Surface deviation contours for 38 actuators arranged in a triangular pattern and bonded to different surface material thickness of 0.05", 0.1" and 0.3" respectively.

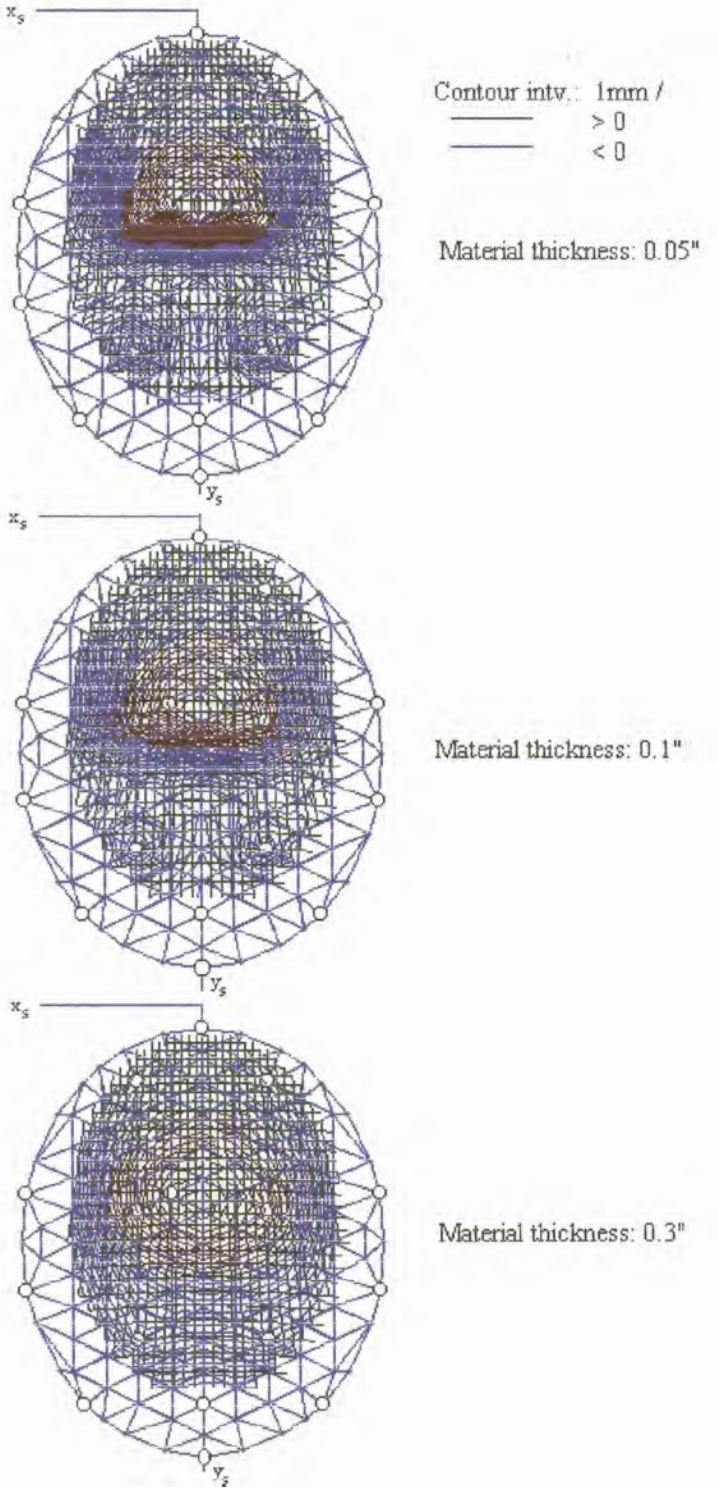

Figure 33 (a) Surface deviation contours for 15 actuators arranged in a rectangular pattern and bonded to different surface material thickness of 0.05", 0.1" and 0.3" respectively.

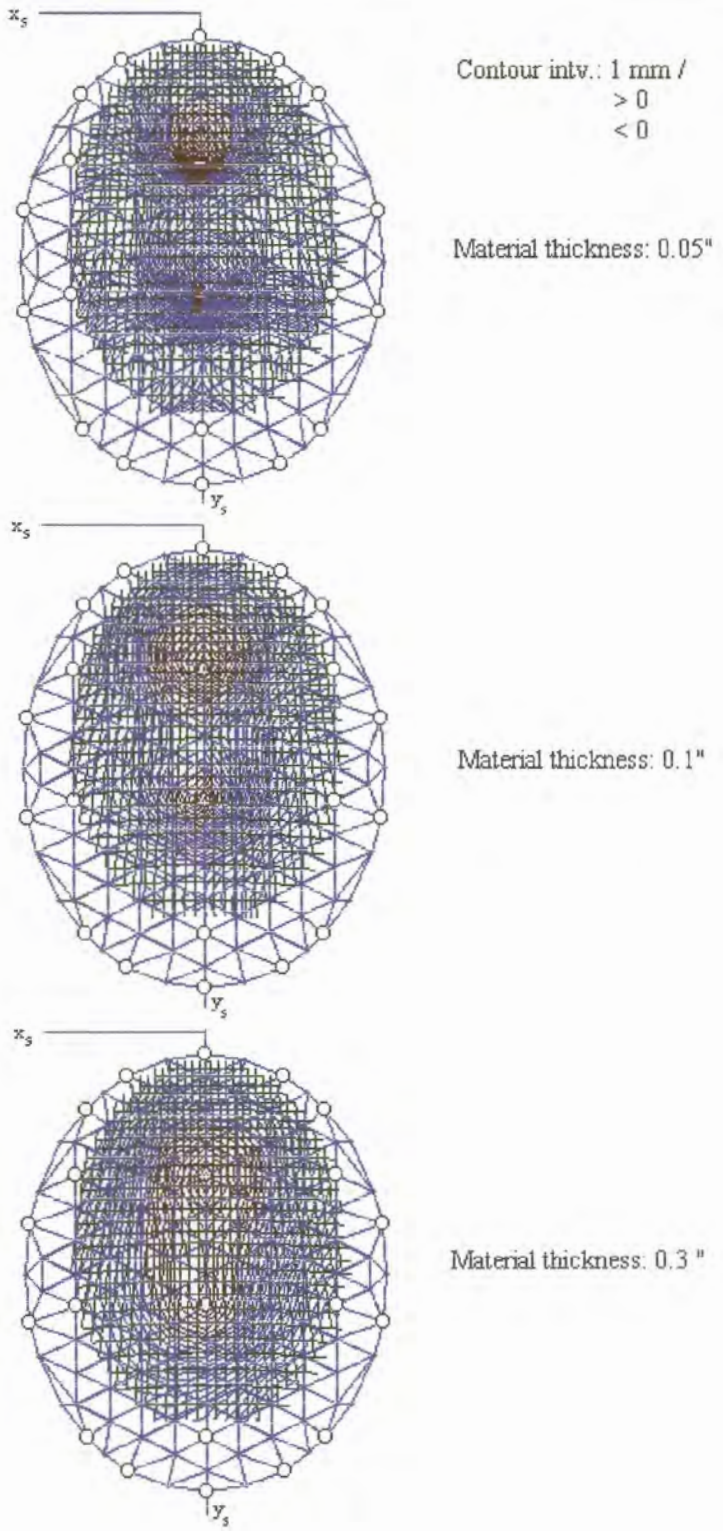

Figure 33 (b) Surface deviation contours for 21 actuators arranged in a rectangular pattern and bonded to different surface material thickness of 0.05", 0.1" and 0.3" respectively.

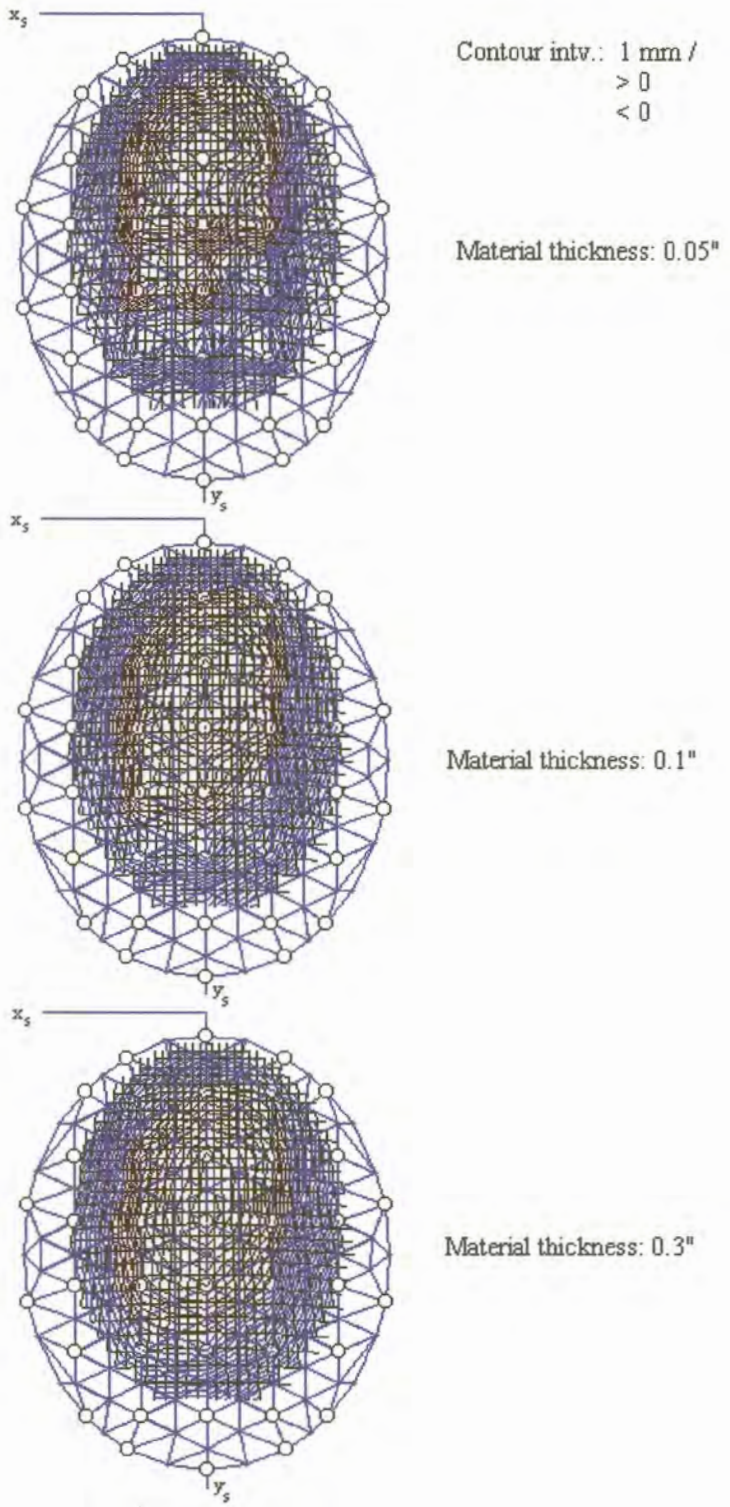

Figure 33 (c) Surface deviation contours for 40 actuators arranged in a rectangular pattern and bonded to different surface material thickness of 0.05", 0.1" and 0.3" respectively.

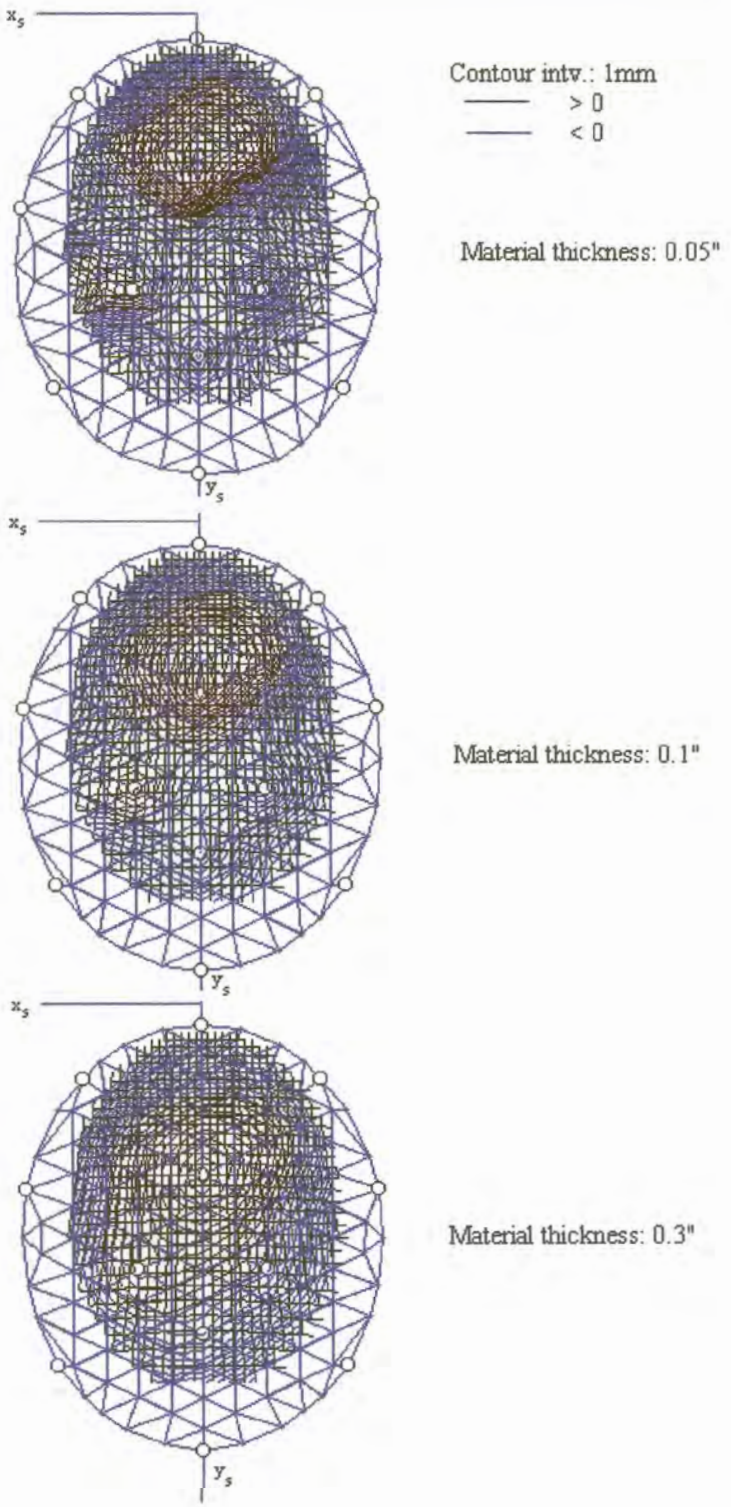

Figure 34 (a) Surface deviation contours for 14 actuators arranged in a radial pattern and bonded to different surface material thickness of 0.05", 0.1" and 0.3" respectively.

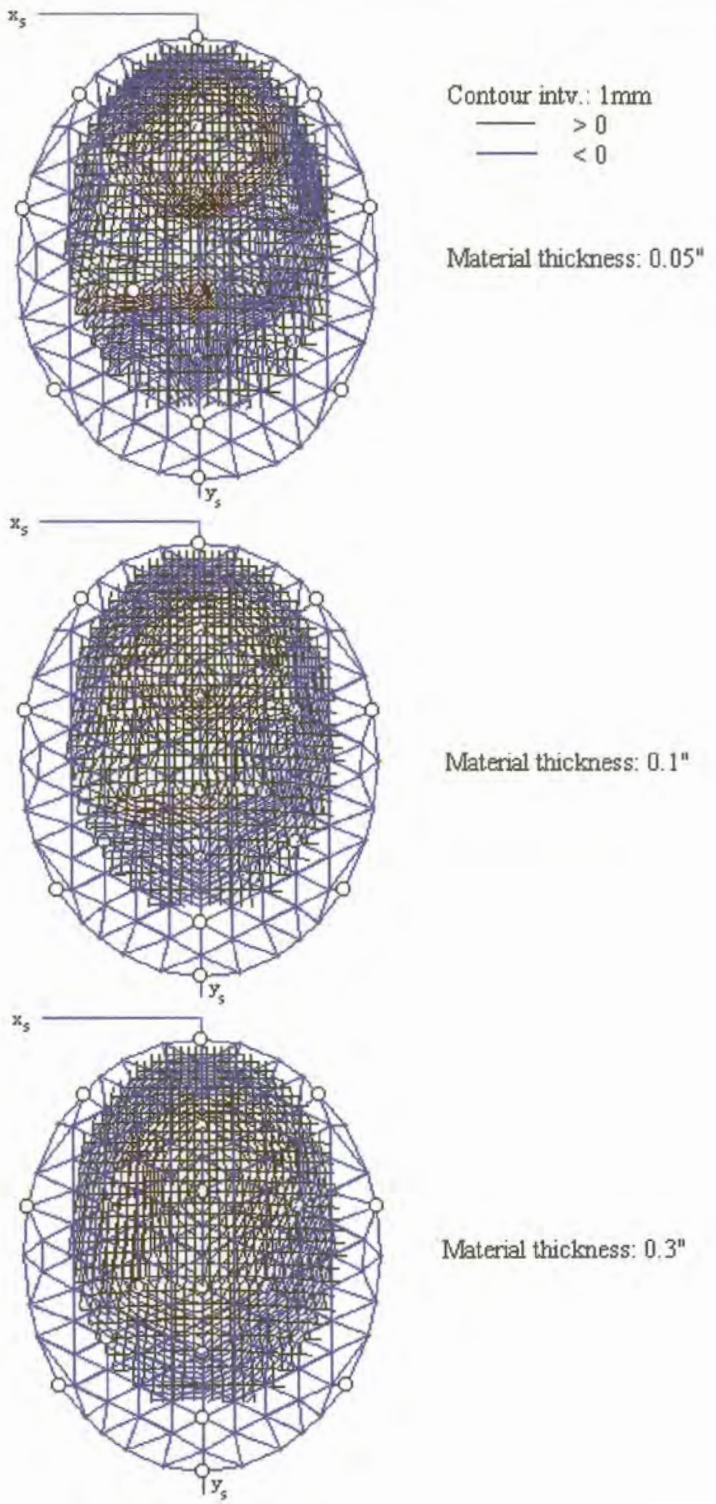

Figure 34 (b) Surface deviation contours for 21 actuators arranged in a radial pattern and bonded to different surface material thickness of 0.05", 0.1" and 0.3" respectively.

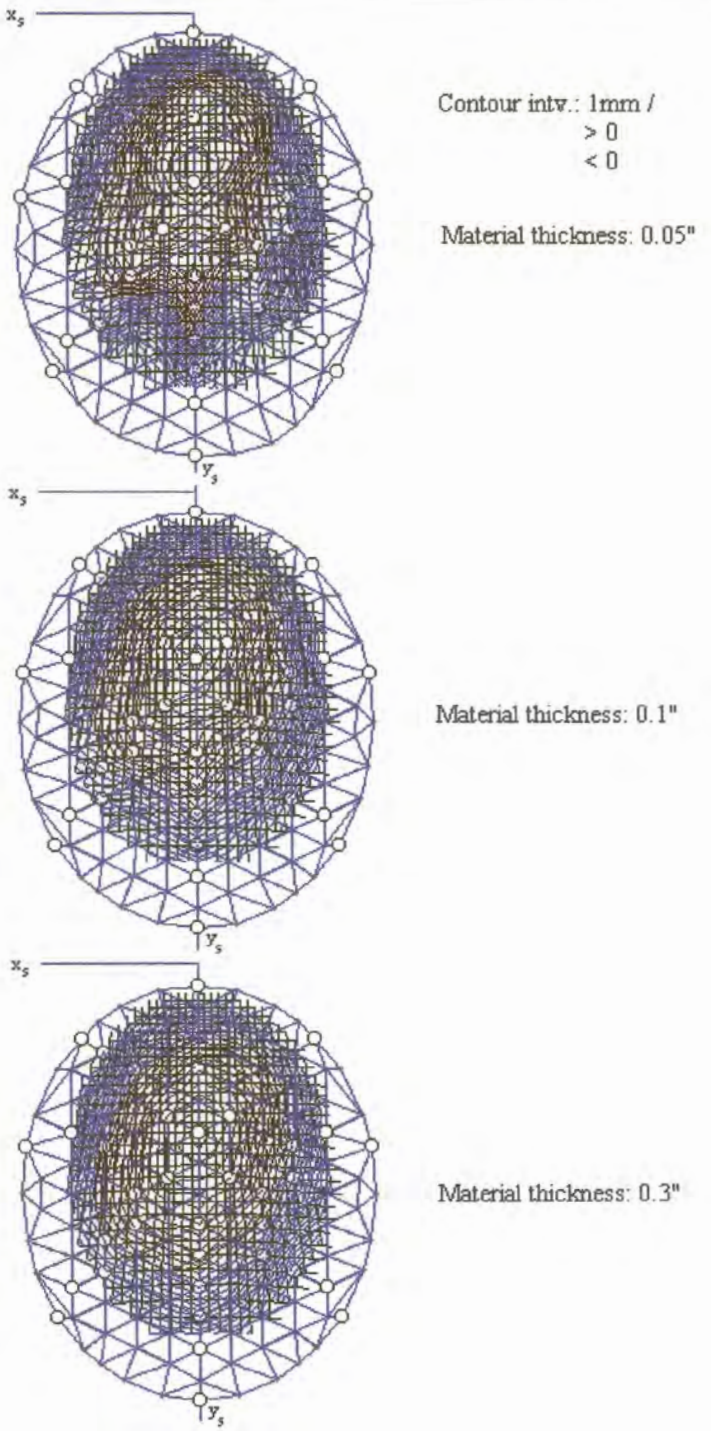

Figure 34 (c) Surface deviation contours for 39 actuators arranged in a radial pattern and bonded to different surface material thickness of 0.05", 0.1" and 0.3" respectively.

5.3. Synthesis of an adjustable elliptical beam using the mechanical FEM surface description

As an example application an adjustable elliptical beam was generated using 38 actuators in the positions shown in figure 31(c) on the subreflector of a dual offset reflector antenna with an unshaped main reflector. In each of the syntheses performed Lexan was used as subreflector material with the following properties

Young's modulus: 0.2×10^{10}

Poisson ratio: 0.334

thickness: 0.2×0.00254m

Figure 31(c) shows the subreflector surface deviation for the 45° case. The co-polarized far-field for 0°, 45° and 90° cases are shown in Figure 35, 36 and 37 respectively. A surface synthesis was first performed on a modified Jacobi polynomial surface expansion to get approximate values for the actuators. After this the FEM diffraction synthesis procedure is applied. This is done because the FEM diffraction synthesis procedure is much slower and the approximate actuator values ensures that a faster convergence is obtained the final solution is found within a few iterations.

This example illustrates the reconfigurability of the antenna system using the adjustable subreflector. This example also shows a practical advantage of the method since a lot of geographical coverage requirements can be satisfied by simple elliptical contour beams [22].

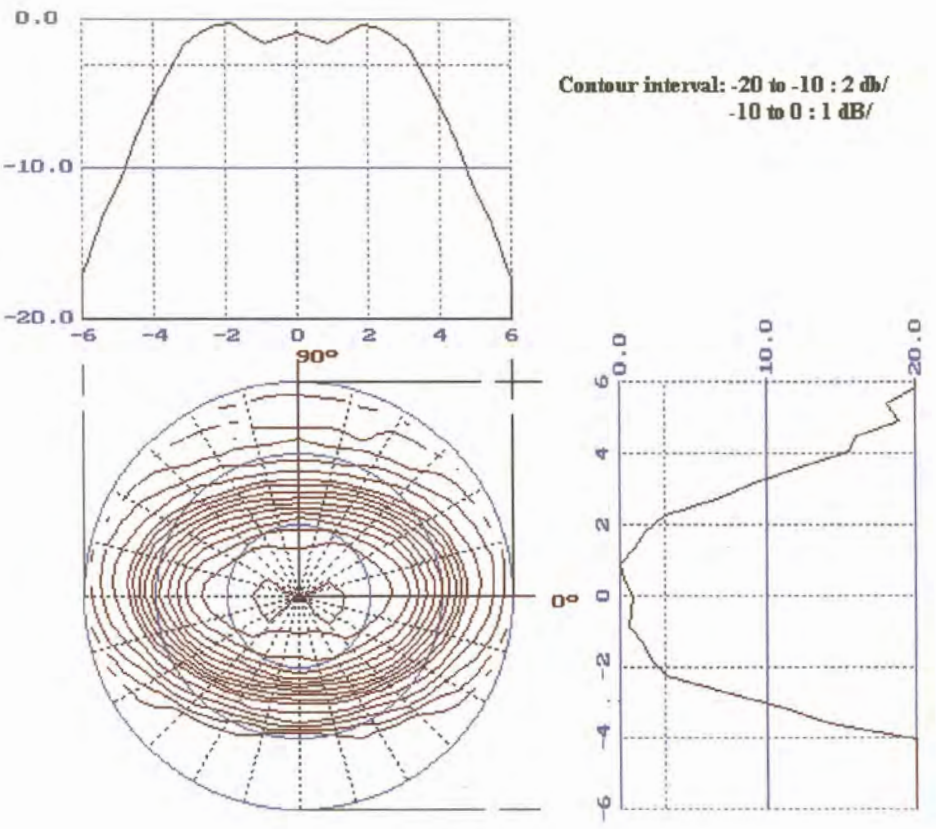

Figure 35. Co-polarized far-field for the 0° elliptical beam case.

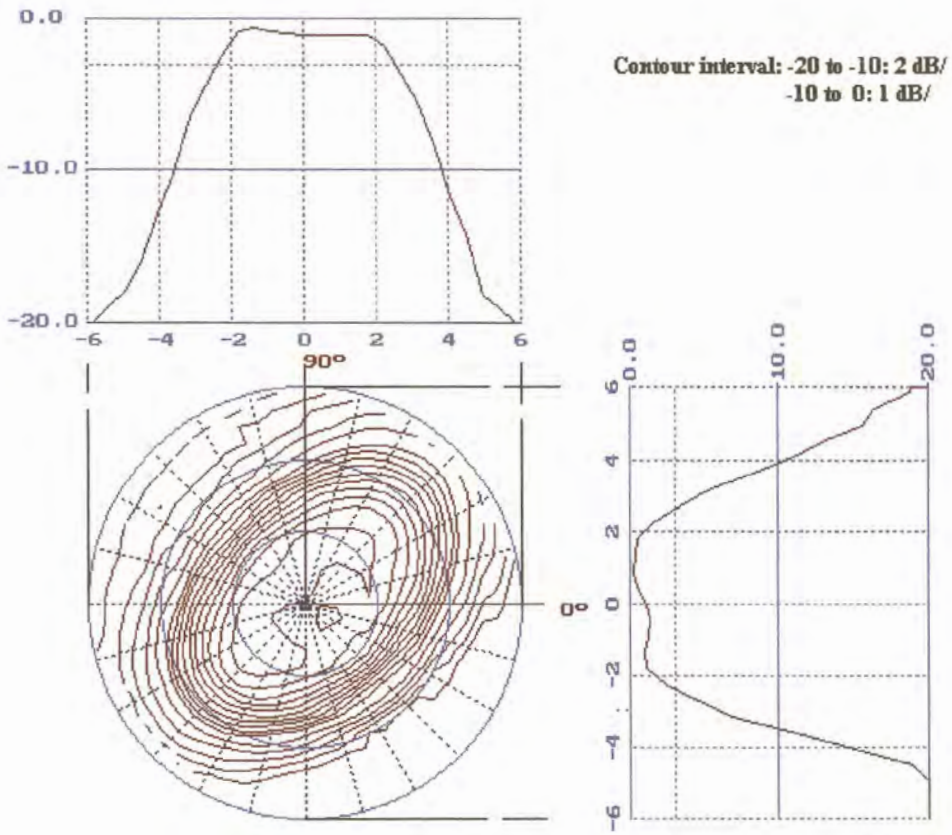

Figure 36. Co-polarized far-field for the 45° elliptical beam case.

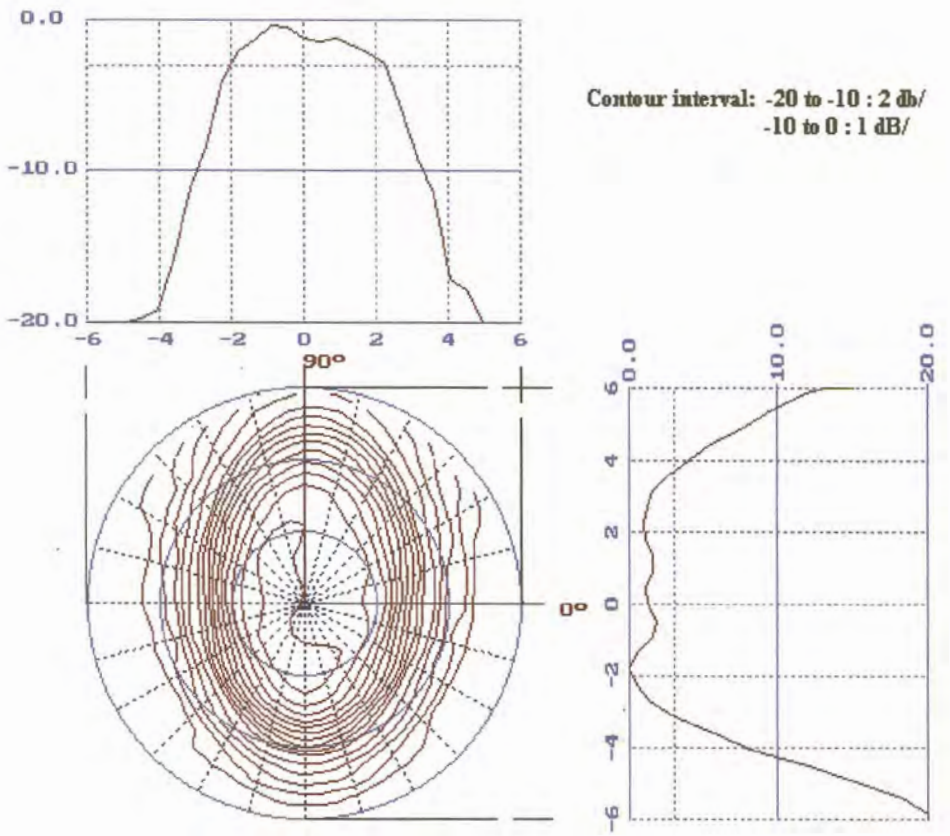

Figure 37. Co-polarized far-field for the 90° elliptical beam case.

5.4. Synthesis of an reconfigurable beam using the mechanical FEM surface description

The FEM diffraction synthesis code is finally re-applied to the three examples described in Chapter 4. In Chapter 4 the actuator placement study is done to determine actuator positions that can achieve the required pattern within a certain cost for the three cases. In the following examples a more general triangular actuator arrangement pattern is used. A reconfigurable beam was generated using 38 actuators in the positions shown in figure 31(c) on the subreflector and the same shaped main reflector as before. As an additional case the same configuration was used to generate an Australian beam.

In each of the syntheses performed Lexan was used as reflector material with the following properties

Young's modulus: 0.2×10^{10}

Poisson ratio: 0.334

thickness: 0.2×0.00254m

The co-polarized far-field for the Brazilian, Southern Africa and Australian beams are shown in Figure 38, 39 and 40 respectively. A surface synthesis was first performed on a modified Jacobi polynomial surface expansion to get approximate initial values for the actuators.

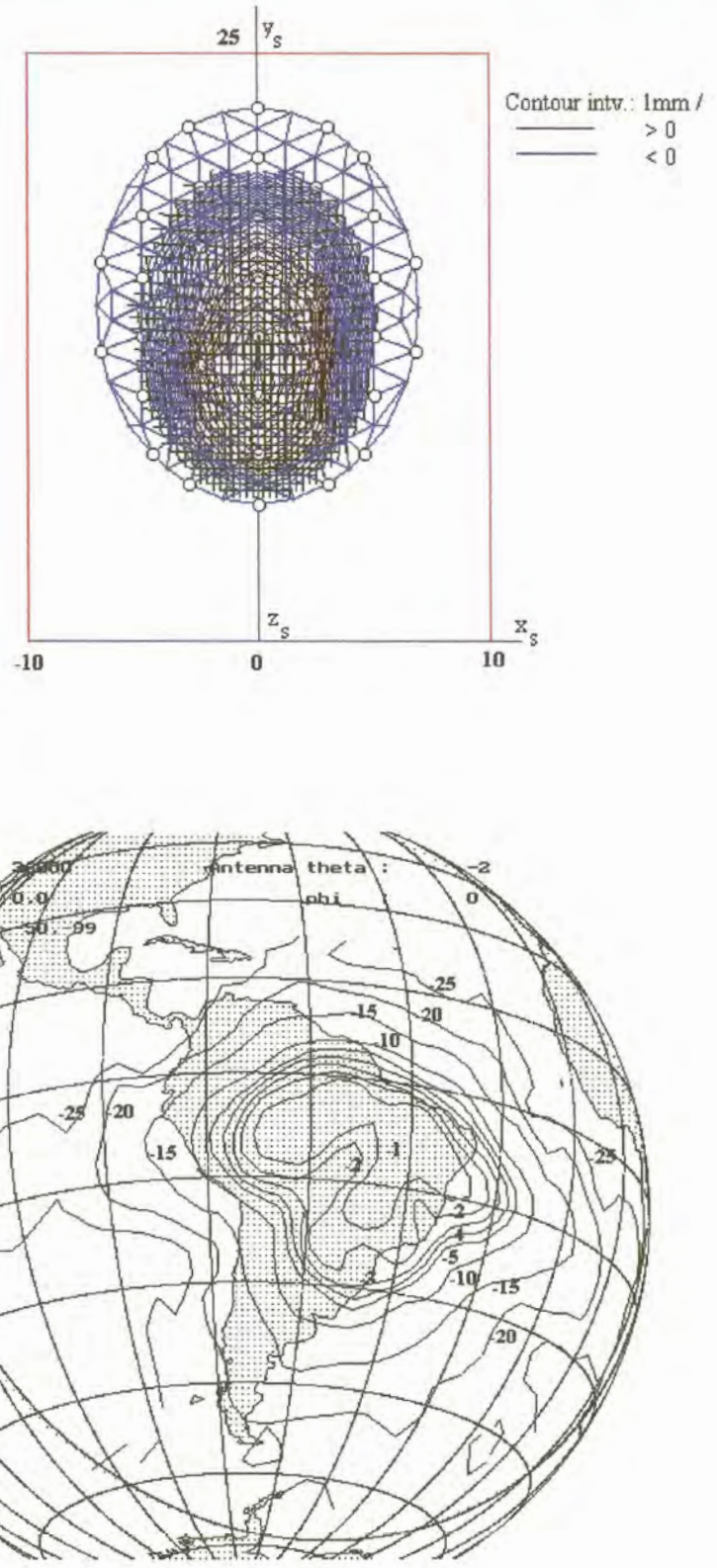

Figure 38. Synthesized subreflector surface and Brazilian co-polarized radiation pattern footprint.

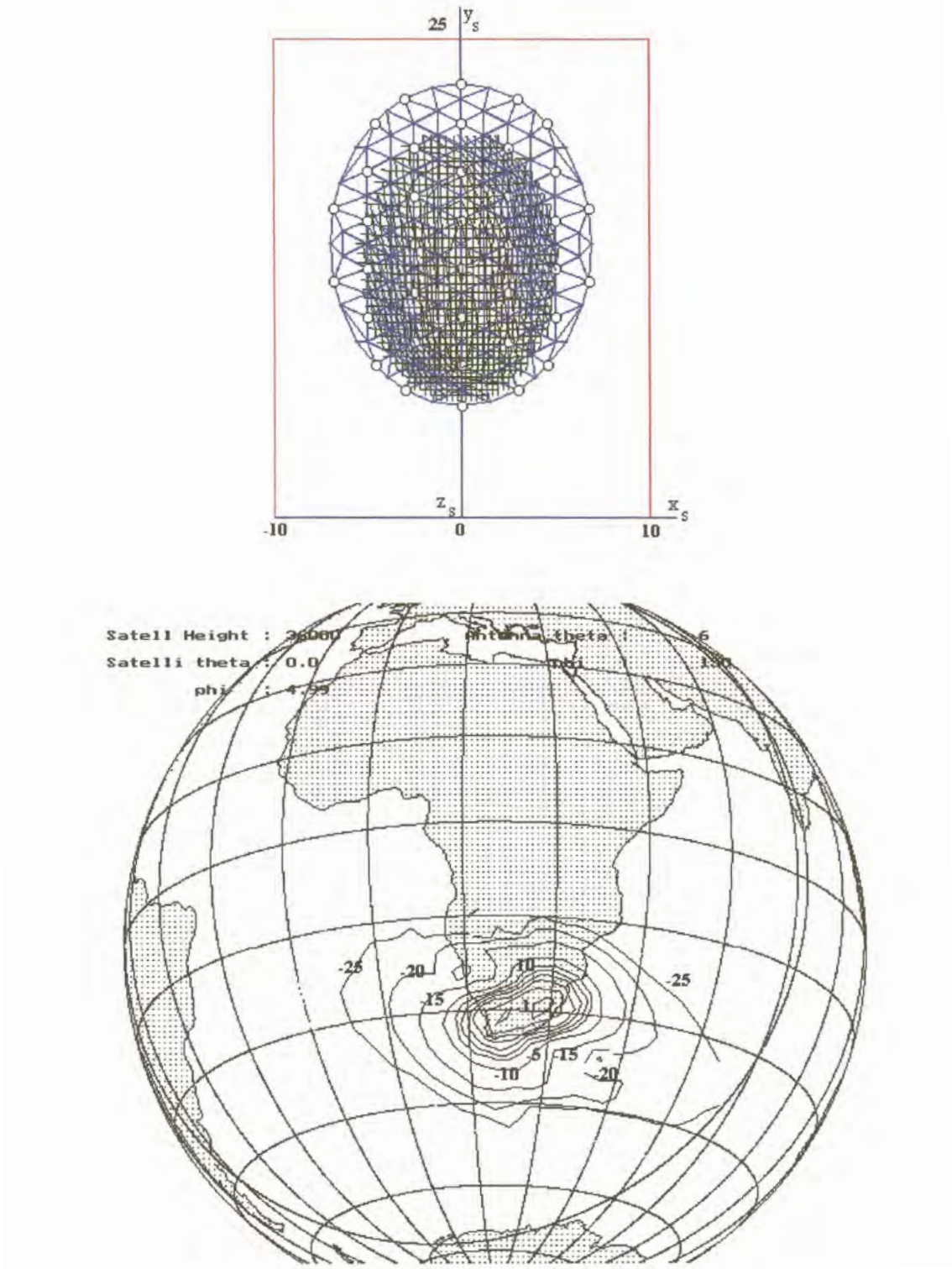

Figure 39. Synthesized subreflector surface and Southern African co-polarized radiation pattern footprint.

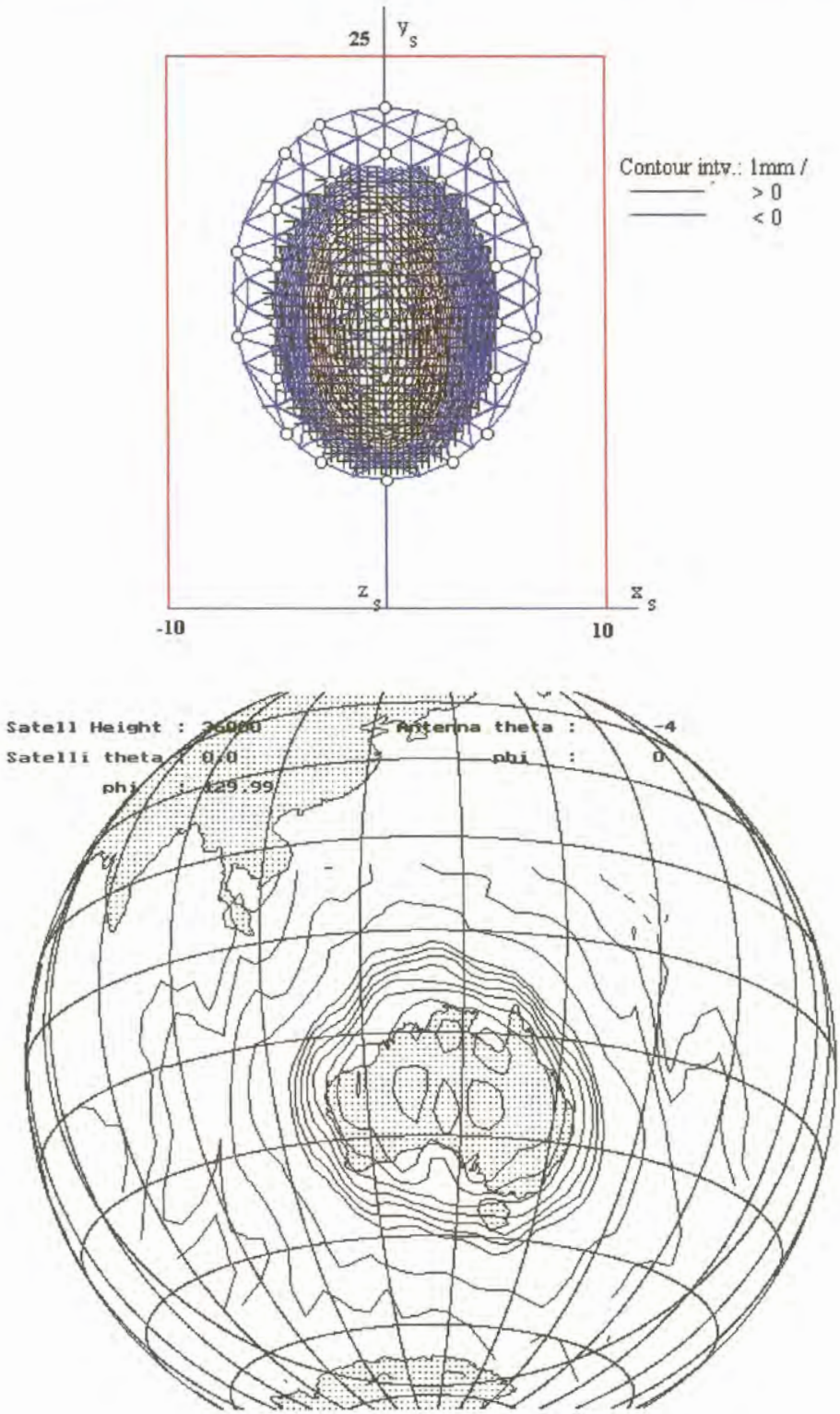

Figure 40. Synthesized subreflector surface and Australian co-polarized radiation pattern footprint.

Chapter 6: Conclusion

In this work the mechanically adjustable surfaces of dual offset reflector antennas have been studied as a possible solution to the problem of creating reconfigurable contour beams for application on geostationary satellites.

A motivation for studying this problem was provided in the introduction. It was stated that reconfigurability of contour beams would increase reflector antenna efficiency and be necessary to comply with FCC regulations on spillover allowed in adjacent geographical regions if the satellite operator or service area changes.

Various algorithms to compute the far-field of a DOSR antenna efficiently were investigated including the Jacobi-Bessel series expansion method and the pseudo sampling technique. The accuracy of the developed code was verified against a PO code developed at the Ohio State University by Rudduck and Lee. A new efficient method to calculate the far-field using a Gaussian beam expansion of the feed pattern to launch and reflect GB's from the main reflector of a front fed offset parabolic reflector, was used to synthesize a CONUS beam [5]. The subreflector analysis was done using UTD. These aspects were discussed in Chapter 2.

Methods to describe the surface using the modified Jacobi polynomial series and Fourier harmonics, which describe a complete orthogonal set over the unit circle, were used to synthesize contour beams. Various methods to describe and optimize the cost function including genetic algorithms and the steepest gradient solver were used.

A reconfigurable DOSR antenna was designed assuming a fixed shaped main reflector and a flexible metal coated surface subreflector. Piezoelectric actuators attached to a support structure will enable reconfiguration of the surface. A family of possible shapes were generated and used to perform an actuator placement study. The mechanical finite element description of the surface was then used to predict the antenna radiation footprint for a few cases [23]. After this it was concluded that the design would be a viable option to consider for future applications.

A mechanical finite element Delphi unit was then developed by Yoon [30] using a shell description of the surface. This unit was added and used in the synthesis software. The surface description could now be made directly in terms of actuator amplitudes and synthesis can thus also be performed directly in terms of the actuator amplitudes. This unique tool for contour beam synthesis is the main contribution of this work and is described in Chapter 5 where a case study to implement a rotating elliptical beam and three shaped beams in reconfigured configuration are also described.

Future work will concentrate on optimizing actuator numbers and placement as well as a method to use piezoelectric strips bonded to the back of the reflector surfaces. This will work will likely be performed under sponsorship from a major aerospace company.